
This manuscript is a preprint. Despite having undergone peer-review, this manuscript has yet to be formally accepted in a journal. Subsequent versions of this manuscript may thus have different content. If accepted, the final version of this manuscript will be available via the ‘*Peer-reviewed Publication DOI*’ link on the right-hand side of this webpage. Please feel free to contact any of the authors directly or to comment on the manuscript using **hypotesis** (<https://web.hypotesis.is/>). We welcome feedback!

1 **Rift-related magmatism influences petroleum systems development in the NE Irish**
2 **Rockall Basin, offshore Ireland**

3
4 Christopher A-L. Jackson

5 Craig Magee*

6 Carl Jacquemyn

7
8 *Basins Research Group (BRG), Imperial College, Prince Consort Road, LONDON, SW7*
9 *2BP, England, UK*

10
11 **Present address: School of Earth and Environment, University of Leeds, Leeds, UK*

12
13 *email: c.jackson@imperial.ac.uk*

14
15 **ABSTRACT**

16
17 Large volumes of hydrocarbons reside in volcanically influenced sedimentary basins. Despite
18 having a good conceptual understanding of how magmatism impacts the petroleum system of
19 such basins, we still lack detailed case studies documenting precisely how intrusive magmatism
20 influences, for example, trap development and reservoir quality. Here we combine 3D seismic
21 reflection, borehole, petrographic, and paleothermometric data to document the geology of
22 borehole 5/22-1, NE Irish Rockall Basin, offshore western Ireland. This borehole (Errigal)
23 tested a four-way dip closure that formed to accommodate emplacement of a Paleocene-to-
24 Eocene igneous sill-complex during continental breakup in the North Atlantic. Two water-
25 bearing turbidite sandstone-bearing intervals occur in the Upper Paleocene; the lowermost
26 contains thin (*c.* 5 m), quartzose-feldspathic sandstones of good reservoir quality, whereas the
27 upper is dominated by poor-quality volcanoclastic sandstones. Paleothermometric data provide
28 evidence for anomalously high temperatures in the Paleocene-to-Eocene succession, suggesting
29 the poor reservoir quality within the target interval likely reflects sill-induced heating, fluid
30 flow, and related diagenesis. The poor reservoir quality also likely reflects the primary
31 composition of the reservoir, which is dominated by volcanic grains and related clays derived
32 from an igneous rock-dominated, sediment source area. Errigal appeared to fail due to a lack of
33 hydrocarbon charge; i.e. the low bulk permeability of the heavily intruded Cretaceous mudstone
34 succession may have impeded vertical migration of sub-Cretaceous-sourced hydrocarbons into
35 supra-Cretaceous reservoirs. Breakup-related magmatism did however drive formation of a
36 large structural closure, with data from Errigal at least proving high-quality, Upper Paleocene
37 deep-water reservoirs. Future exploration targets in the NE Irish Rockall Basin include: (i)

38 stratigraphically trapped, Paleocene-to-Eocene deep-water sandstones that onlap the flanks of
39 intrusion-induced forced folds; (ii) structurally trapped, intra-Cretaceous deep-water
40 sandstones incorporated within intrusion-induced forced folds; and (iii) more conventional,
41 Mesozoic fault-block traps underlying the heavily intruded Cretaceous succession (e.g.
42 Dooish). Similar plays may exist on other continental margins influenced by break-up
43 magmatism.

44

45 **INTRODUCTION**

46

47 Stretching and thinning of the lithosphere during continental breakup, or elevated mantle
48 potential temperatures (T_p), drive melting of asthenospheric mantle (e.g. Jerram & Widdowson,
49 2005; Allen & Allen, 2013; Hole & Millett, 2016). Magma formed during continental breakup
50 may stall during its ascent to the Earth's surface, intruding the crust in the form of igneous sills
51 and dykes. Because continental stretching precedes breakup, igneous intrusions are particularly
52 common in some of the world's most prolific hydrocarbon provinces (e.g. offshore circum-
53 Atlantic, e.g. Smallwood and Maresh, 2002; Rohrman, 2007; Thomson & Hutton, 2004; Archer
54 et al., 2005; Magee et al., 2014; Schofield et al., 2017; NW Shelf of Australia, Reeckman and
55 Mebberson, 1984; Magee et al., 2013a,b; McClay et al., 2013; Rohrman, 2015; Magee et al.
56 2017). Petroleum systems in these provinces are commonly assumed to be negatively impacted
57 by breakup-related magmatism. For example, sill and dyke intrusion can cause: (i) physical
58 compartmentalization of stratigraphy, leading to dissection of reservoirs, or separation of
59 source and reservoir rocks by impermeable sills and dykes (e.g. Thomaz Filho et al., 2008;
60 Senger et al., 2015; Eide et al., 2017; Grove et al., 2017); (ii) initiation of hydrothermal systems,
61 with the local flow of anomalously hot fluids driving diagenesis at shallow depths and causing
62 a reduction in reservoir quality (e.g. Grove et al., 2017); (iii) overmaturation of source rocks
63 (e.g. Schutter, 2003; Rohrman, 2007; Holford et al., 2013; Schofield et al., 2018) (see also
64 reviews by Schutter, 2003 and Senger et al., 2017); and (iv) operational (i.e. drilling) issues
65 related to the pressure state of the intrusion and encasing rocks, or the high strength of the
66 intrusions, both of which can lead to enhanced risk for equipment and personnel, and can lead
67 to costly 'non-productive time' (e.g. Millet et al., 2016; Iyer et al., 2017; Mark et al., 2018).
68 However, the discovery and production of hydrocarbons in association with igneous rocks
69 demonstrate breakup-related magmatism may positively impact petroleum system development
70 by: (i) causing the formation of structural and stratigraphic traps due to forced folding (e.g.
71 Reeckmann and Mebberson, 1984; Smallwood and Maresh, 2002; Schutter, 2003; Wu et al.,
72 2006; Rohrman, 2007; Magee et al., 2013a; Egbeni et al., 2014; Schmiedel et al., 2017; Mark
73 et al., 2017; Schofield et al., 2018; Magee et al., 2019); (ii) creating a network of interconnected,
74 potentially high-permeability intrusions that may act as either reservoirs (e.g. Reeckmann and

75 Mebberson, 1984; Gu et al., 2002; Smallwood and Maresh, 2002; Schutter, 2003; Rohrman,
76 2007; Delpino & Bermúdez, 2009; Farooqui et al., 2009; Wang et al., 2012; Witte et al., 2012;
77 Egbeni et al., 2014; Bischoff et al., 2017), or as conduits that allow hydrocarbons to migrate
78 from source rocks to reservoir rocks (e.g. Rateau et al., 2013; Rodriguez Monreal et al., 2009;
79 Senger et al., 2015; Schofield et al., 2017; Mark et al., 2018); (iii) increasing the reservoir
80 quality of encasing host rock (e.g. by dolomitization; see Jacquemyn et al., 2014); (iv) forming
81 low-permeability seals (e.g. Schutter, 2003; Rodriguez Monreal et al., 2009; Wang et al., 2012);
82 (iv) locally maturing otherwise regionally immature source rocks (e.g. Svensen et al., 2004;
83 Wang et al., 2012; Holford et al., 2013; Aarnes et al., 2015; Iyer et al., 2017; Muirhead et al.,
84 2017; Senger et al., 2017); and (v) acting a seals to hydrocarbons trapped in more conventional
85 reservoirs (e.g. Schutter, 2003; Wu et al., 2006; Thomaz Filho et al., 2008; Holford et al., 2013).
86 Our understanding of how magmatism impacts petroleum systems development in volcanic
87 basins has grown in recent years, yet we still lack detailed case studies documenting the precise
88 influence intrusive magmatism has on, for example, trap development and reservoir quality (see
89 reviews by Schutter, 2003, Rohrman, 2007, and Senger et al., 2017). Even with a relatively
90 advanced conceptual framework within which to risk prospects and devise field development
91 plans, hydrocarbon exploration and development in volcanic basins remains challenging (Mark
92 et al., 2017; Schofield et al., 2018).

93 To help improve our understanding of how breakup-related magmatism impacts
94 petroleum systems development along continental margins, we provide a detailed post-well
95 analysis of exploration borehole 5/22-1, which tested the Errigal prospect, NE Irish Rockall
96 Basin (PEL 6/97), offshore western Ireland (Fig. 1). This borehole was drilled by Enterprise
97 Energy Ireland Ltd and partners in 2001, targeting a large (*c.* 77 km²; revised to 52 km² post-
98 drilling; see Supplementary Item 1) dome (i.e. four-way dip closure) situated *c.* 42 km NNW
99 of the Dooish discovery (12/2-1), which was drilled in 2003 and represents the first commercial
100 hydrocarbon discovery in the NE Irish Rockall Basin (Figs 1 and 2). Borehole 5/22-1 took 26
101 days to drill to a total depth of 4070 m, in water depths >1500 m. The primary and secondary
102 objectives were Upper and lower Paleocene deep-water sandstone, respectively, sealed by latest
103 Paleocene and Eocene mudstone (Fig. 1C). The prognosed trap and reservoir-seal pairs are
104 underlain by an extensive, breakup-related (i.e. earliest Paleocene-to-early Eocene), igneous
105 sill-complex primarily intruded into Cretaceous mudstone (Figs 2 and 3) (Magee et al., 2014).
106 Oil was predicted to be the main hydrocarbon phase, sourced from Lower Jurassic (intra-rift)
107 or Upper Jurassic (syn-rift) marine mudstone. The well reached Late Cretaceous rocks (Figs 1C
108 and 2) and, despite penetrating a sandstone-bearing Eocene and upper Paleocene sequence, was
109 plugged and abandoned as a dry hole, with only very minor traces of hydrocarbons being
110 recorded in the target interval.

111 Although the failure of Errigal seemingly cast doubt on the prospectivity of this play
112 type in at least this particular part of the NE Irish Rockall Basin, data acquired during drilling
113 provide an excellent opportunity to assess the role breakup magmatism had on petroleum
114 systems development in this and possibly other volcanically influenced basins. We begin by
115 briefly summarizing the tectono-magmatic and petroleum systems framework of the NE Irish
116 Rockall Basin, before using 3D seismic reflection and borehole data to constrain the structural,
117 stratigraphic, and magmatic context of Errigal. We place particular emphasis on the origin and
118 timing of the trap, and how this relates to breakup magmatism. We then use a range of
119 predominantly pre-2004, now-released data, generously provided by the Department of
120 Communications, Energy and Natural Resources (Petroleum Affairs Division), Ireland to: (i)
121 describe and interpret spatial and temporal changes in the thickness and quality of the main
122 Paleocene reservoir target (e.g. via final well reports, petrographic analysis); and (ii) constrain
123 the paleothermometric evolution via fluid inclusion microthermometry (FIM), vitrinite
124 reflectance (VR) and apatite fission track analysis (AFTA) data from the basin, with a view as
125 to how this might relate to the inferred magmatic events and observed reservoir quality. In
126 addition to improving our understanding of petroleum systems development along the deep-
127 water margin of western Ireland and the UK (e.g. the Faroe-Shetland Basin and UK Rockall
128 Basin; *sensu* Schofield et al., 2018), the results of our study can also help us better understand
129 the challenges associated with similar prospects identified in other volcanically influenced
130 basins worldwide.

131

132 **GEOLOGICAL SETTING AND PETROLEUM SYSTEM ELEMENTS**

133

134 The Rockall Basin is located along the NE Atlantic continental margin (Fig. 1). It is one of
135 several deep-water (i.e. water depth of up to 1800 m) rifts that formed during initial opening of
136 the North Atlantic (e.g. Doré et al. 1999; Naylor & Shannon 2005; Hansen et al. 2009). In the
137 NE Irish Rockall Basin the earliest phase of breakup-related extension occurred in the Permo-
138 Triassic ('syn-rift I' of Magee et al., 2014; Figs 1C and 2), with a second phase occurring in the
139 Middle-to-Late Jurassic ('syn-rift II' of Magee et al., 2014; Figs 1C and 2) (e.g. Doré et al.
140 1999; Naylor & Shannon 2005; Tyrell et al. 2010). Marine mudstone source rocks may occur
141 in the Lower (Lias equivalent) and Upper (Kimmeridge Clay Formation equivalent) Jurassic
142 successions, although this remains speculative due to a lack of deep borehole data (e.g. Doré et al.
143 al. 1999; Tyrell et al. 2010; see also discussion by Schofield et al., 2018 on the UK Rockall
144 Basin).

145 Northwards propagation of North Atlantic seafloor spreading during the late Early
146 Cretaceous (Aptian-to-Albian) led to NW-SE-oriented extension and a third phase of rifting in
147 the Rockall Basin (Doré et al. 1999). A deep marine, mudstone-dominated succession was

148 deposited within the deepening rift during this period of Early Cretaceous stretching ('syn-rift
149 III' of Magee et al., 2014; Figs 1C and 2) (Naylor & Shannon 2005). Early Cretaceous extension
150 was superseded by Late Cretaceous-to-Paleogene post-rift thermal subsidence. During the Late
151 Paleocene and Eocene, deposition of deep-marine mudstone was intermittently interrupted by
152 the deposition of deep-water sandstone derived from a volcanic terrain emplaced during the
153 immediately preceding (and in places broadly synchronous) period of breakup-related
154 magmatism (see also Naylor & Shannon 2005; Haughton et al. 2005).

155 Paleocene deep-water sandstone and Eocene mudstone represented the prognosed
156 reservoir and seal, respectively, for the Errigal prospect. Lower and Upper Jurassic marine
157 mudstone, in addition to underlying Carboniferous coals, represent potential source rocks. The
158 Dooish discovery (estimated to contain recoverable volumes of c. 256 bcf and c. 17 mmbbls
159 45° API condensate) contains a Mesozoic (Triassic-to-Middle-Jurassic), marginal marine
160 sandstone reservoir located in a rift-related fault block, demonstrating the presence of a working
161 petroleum system within the NE Irish Rockall Basin (Fig. 1C and 2).

162

163 **BREAKUP RELATED MAGMATISM AND ASSOCIATED DEFORMATION**

164

165 Late Cretaceous-to-Early Eocene, breakup-related magmatism is common along the NE
166 Atlantic Margin, manifesting as flood basalt lava flows, sill-complexes and volcanic centres
167 (North Atlantic Igneous Province; Fig. 1A). The products of this magmatism have been
168 identified and described using seismic reflection and borehole data from the UK (Thomson &
169 Hutton, 2004; Archer et al. 2005) and NE Irish Rockall basins (Fernandes, 2011; Magee et al.,
170 2014). Igneous intrusions, in particular sills, are common in the NE Irish Rockall Basin, being
171 expressed in seismic reflection data as very high amplitude, typically strata-discordant
172 reflections (Fig. 2) (Magee et al., 2014). The presence of intrusive igneous material in the NE
173 Irish Rockall Basin is confirmed by well 12/2-1, which penetrates a c. 14 m thick dolerite sill
174 in upper Paleocene mudstones overlying the Dooish discovery (e.g. Figs 1C and 4).

175 An extensive network of large, interconnected, saucer-shaped and inclined sills, which
176 individually are up to 12.4 km long and cross-cut 1.8 km of stratigraphy, are developed north
177 of Dooish (Fig. 2) (Magee et al., 2014). These intrusions are most densely stacked directly
178 beneath the dome drilled by 5/22-1 and are largely hosted within Upper Cretaceous mudstone,
179 although a few extend upwards into the reservoir-bearing Paleocene succession (Fig. 5; cf. the
180 Rockall (e.g. Schofield et al., 2018) and Faroe-Shetland (e.g. Mark et al., 2017) basins). Based
181 on: (i) the fact that the sills are most densely stacked below the dome apex; and (ii) the
182 observation that the Paleocene to Lower Eocene succession onlaps onto and thins across the
183 dome (Figs 2 and 5), Magee et al. (2014) argue the dome (forced fold) formed to accommodate

184 incremental emplacement of magma over a *ca.* 15 Myr period earliest Paleocene-to-early
185 Eocene (Danian-to-Ypresian).

186

187 **DATASET**

188

189 Our dataset comprises: (i) digital seismic reflection and borehole data, much of which was
190 presented by Magee et al. (2014) in their study of the tectono-magmatic history of the NE Irish
191 Rockall Basin; and (ii) ‘analogue’ data derived from now-released reports detailing previously
192 confidential analyses undertaken immediately after drilling of 5/22-1 (Errigal) in 2001 and
193 12/2-1 (Dooish) in 2003 (see Supplemental Items 1-6, which are available upon request from
194 the Department of Communications, Climate Action & Environment (Petroleum Affairs
195 Division), Ireland via [https://www.dccae.gov.ie/en-ie/natural-resources/topics/Oil-Gas-
196 Exploration-Production/data/Pages/Data.aspx](https://www.dccae.gov.ie/en-ie/natural-resources/topics/Oil-Gas-Exploration-Production/data/Pages/Data.aspx)).

197

198 **Seismic reflection data**

199

200 The seismic dataset comprises a zero-phase, time-migrated, 3D seismic reflection survey that
201 covers 2400 km². Inline (N-S) and crossline (E-W) spacing is 12.5 m (Fig. 1B). These data are
202 displayed with a normal polarity, whereby a downward increase and decrease in acoustic
203 impedance corresponds to a positive (red) and negative (blue) reflection, respectively (Fig. 2).
204 We mapped four horizons: (i) Top Hauterivian (KH) (intra-syn rift III); (ii) Top Cretaceous (K)
205 (near base reservoir); (iii) Top Paleocene (P) (near top reservoir); and (iv) Top Lower Eocene
206 (E) (intra-post rift). Where data quality allows, we locally define and map an additional seismic
207 horizon that corresponds to the intra-Cenomanian (KC) and likely demarcates the boundary
208 between syn-rift III and younger post-rift rocks (Fig. 2).

209 Interval velocities of 2250 metres per second (m s⁻¹) (seabed to E), 3220 m s⁻¹ (E to K),
210 and 4000 m s⁻¹ (below K) were calculated from borehole data. Given that the dominant seismic
211 frequency is *c.* 25 Hz in the stratigraphic interval of interest, interval velocities of 3220–4000
212 m s⁻¹ suggest that the vertical resolution of the seismic data ranges from *c.* 32–40 m for the host
213 rock succession (see Magee et al., 2014).

214

215 **Borehole and petrophysical data**

216

217 We use data from two boreholes (5/22-1; Errigal, and 12/2-1; Dooish) to constrain the age and
218 lithology of the seismically mapped stratigraphic units (Figs 2 and 5). Both boreholes contain
219 a full suite of well-log data, including gamma-ray (GR), density (RHOB), and velocity (DT)
220 logs. Composite logs (Supplemental items 2 and 6) and cuttings data (see information provided

221 in Supplemental items 1, 2 and 6) were available for 5/22-1 and 12/2-1; a final well report was
222 also available for 5/22-1 (Supplemental Item 1).

223 As documented in the final well report for 5/22-1, Volume-of-clay (Vcl) determination
224 was difficult in the Upper Palaeocene interval of interest. A GR-based approach yielded results
225 that were not consistent with cuttings and sidewall core descriptions, or other log responses
226 such as spontaneous potential (SP). More consistent results were gained by using the separation
227 in the RHOB and DT logs, or from the SP measurements; the former was eventually used to
228 constrain Vcl given it had a higher vertical resolution (i.e. sampling interval).

229 Porosity was determined from the RHOB log using an equation that has been modified
230 to account for the high non-net clay component:

231

$$232 \quad \Phi = \frac{(RHOMA - RHOLOG) - Vcl (RHOMA - RHOCL)}{RHOMA - RHOFI}$$

233

234 where RHOMA=rock density in g cm³, RHOLOG=Y, RHOCL=Z, and RHOFI=A (see
235 Supplementary Item 1). Note that core grain density was not available for the Paleocene interval
236 of interest, thus a value of 2.67 g cm³ was used based on core data from analogues rock types
237 penetrated in boreholes west of Shetland.

238

239 **Petrographic data**

240

241 Thin section descriptions (Fig. 6), point-counted petrological descriptions (Table 1 in
242 Supplementary Item 1) and SEM analyses (raw data not available) were undertaken for 13
243 sidewall core samples; 11 of these samples were also studied by whole rock X-ray diffraction
244 (Table 2 in Supplementary Item 1). X-ray diffraction samples for the Upper Paleocene interval
245 of interest were taken from between 3470-3925 m (white and greyscale dots in Fig. 4).

246

247 **Paleothermometric data**

248

249 Paleothermometric data are provided in the form of several reports documenting the methods
250 and analyses undertaken by the operator company and contractors soon after completion of
251 5/22-1 (Errigal) in 2001. The paleothermometric analysis presented here includes the results of
252 FIM (Supplementary Item 3), VR and AFTA analysis (Supplementary Item 4).

253

254 **PALEOCENE RESERVOIR DISTRIBUTION, QUALITY AND PROVENANCE**

255

256 We here describe and interpret the distribution and quality, and infer the possible provenance
257 of, the upper Paleocene deep-water sandstones penetrated in 5/22-1 (Errigal) and 12/2-1
258 (Dooish) (Fig. 4; see also Supplementary items 1-3).

259

260 **5/22-1 (Errigal)**

261

262 5/22-1 penetrated two deep-water turbidite sandstone-bearing intervals (upper Paleocene 1 and
263 2) in the primary, upper Paleocene objective; no sandstones were developed in the secondary,
264 lower Paleocene objective (Fig. 4; see also Supplementary items 1 and 2).

265 The upper sandstone-bearing interval (3505-3619 m; labelled 'Pal. 1' in Fig. 4) is *c.*
266 114 m thick and contains 1-4 m thick beds of generally well-sorted, subangular-to-subrounded,
267 very fine-to-locally medium-grained volcanoclastic sandstones that contain "mafic" grains (Fig.
268 6A and B; see also Supplementary items 1 and 2). Petrophysical analysis of the upper interval,
269 using a volume-of-clay (Vcl) cut-off of 50% (i.e. Vcl >50% is non-net sand) and a 10% porosity
270 cut-off for net-reservoir, indicates that the net reservoir content (1.4 m) and resulting net-to-
271 gross (N:G) of the upper interval is very low (<1%) (Supplementary Items 1 and 2; see also
272 Fig. 4).

273 Thin section (Fig. 6B) and SEM analysis (Supplementary Item 1) reveals that chlorite
274 and chlorite smectite (46% of the bulk rock volume), smectite and zeolites (analcime; 18% of
275 the bulk rock volume) are the main cement phases, filling pores and clogging pore throats.
276 Pyrite, gypsum and small amounts of carbonate and authigenic feldspar are also observed, in
277 addition to weathered volcanic glass fragments and tuffaceous material. Authigenic quartz is
278 lacking, reflecting the lack of primary detrital quartz or inhibition of quartz precipitation due to
279 the presence of chlorite (Supplementary items 1 and 2) (e.g. Berger et al., 2009). Despite locally
280 having a relatively high porosity (21%), reservoir quality in the upper interval is rather poor,
281 with porosity being dominated by intercrystalline and grain dissolution-related microporosity
282 (Supplementary Item 1). We note that these somewhat surprisingly high porosity values may
283 be erroneous, given they were calculated using neutron logs that would record water bound to
284 the (hydrous) clay minerals, and not necessarily water within the pore spaces (e.g. Broglia &
285 Ellis, 1990). As such, the porosity of this volcanoclastic sandstone in Paleocene 1 could be
286 substantially lower.

287 The lower sandstone-bearing interval (3619-3930 m; labelled 'Pal. 2' in Fig. 4) is *c.*
288 311 m thick and contains scattered, generally thinner (<4 m and more commonly 1-2 m thick),
289 volcanoclastic sandstones, of similar composition to the upper interval (see also Supplementary
290 items 1 and 2). However, towards its base, this interval contains two *c.* 5 m thick, quartzose-
291 feldspathic sandstones (3916-3926 m; Fig. 4). These sandstones are fine-to-medium-grained
292 and moderately well-sorted, with individual grains being subangular. Note that, although

293 petrographically distinct from overlying, volcanoclastic sandstones, the quartzose-feldspathic
294 sandstones were originally assigned to 'Pal. 2' in the post-drilling reports; for consistency we
295 retain this nomenclature here (Fig. 4; see also Supplementary Item 1).

296 Thin-section (Fig. 6C) and SEM (Supplementary Item 1) analysis indicate that the
297 quartzose-feldspathic sandstones have distinctly different cement phases and porosity systems
298 to the immediately overlying sandstones or those within upper Paleocene 1. First, they lack
299 pore-filling and pore throat-bridging chlorite, chlorite smectite and zeolite, instead containing
300 relatively limited amounts of illite and kaolinite, in addition to some carbonate cements (Fig.
301 6C); volcanic glass fragments are also absent. Second, well-connected interparticle
302 macroporosity, instead of poorly developed intercrystalline and grain dissolution-related
303 microporosity, is present in these sandstones (cf. Figs 6B and C; see also Supplementary Item
304 1). Petrophysical analysis of the entire lower interval, using the same criteria as the upper
305 interval, indicates that the net sand content (8.1 m) and N:G is very low (c. 3%) (see Fig. 4),
306 although the porosity of the basal quartzose-feldspathic sandstones is generally quite good (up
307 to 16%) (Supplementary Item 1).

308

309 **12/2-1 (Dooish)**

310

311 Because the Triassic and Jurassic succession was the target of well 12/2-1, only a completion
312 log is available for the Paleocene succession (Supplementary Item 5). These data indicate that
313 the >500 m thick upper Paleocene succession is mudstone-dominated; however, in its lower c.
314 150 m, it contains several 1.5-12 m thick, volcanoclastic sandstone beds in an overall silty,
315 relatively low N:G interval (c. 20%) (Fig. 4; see also Supplementary Item 5). Texturally, these
316 sandstones are fine-to-coarse-grained, angular to subrounded, and very well-sorted.
317 Compositionally these sandstones are composed of quartz, volcanic lithics and volcanic glass
318 (Supplementary Item 5), similar to the volcanic sandstone described in the upper part of 5/22-
319 1 (Pal. 1). In the upper part of the upper Paleocene succession, a few 1-3 m thick beds of
320 medium-to-coarse-grained, very well-sorted, subangular-to-subrounded sandstones occur (Fig.
321 4; see also Supplementary Item 5). These sandstones are compositionally very different to those
322 encountered lower in the succession, being quartz-rich and lacking volcanic lithics or volcanic
323 glass. These upper sandstones are similar to the quartzose-feldspathic beds present near the
324 base of the upper Paleocene succession in 5/22-1 (Pal. 2).

325

326 **Interpretation and comparison of 5/22-1 (Errigal) and 12/2-1 (Dooish)**

327

328 Given the regional setting of the NE Atlantic during the late Paleocene, it is likely that the mafic
329 volcanic grains within the upper Paleocene volcanoclastic sandstones penetrated in 5/22-1

330 (Errigal) (Pal. 1) were sourced from relatively distal volcanic terrains forming part of the British
331 and Irish Paleogene Igneous Province. Onshore elements of this province lay to the E (i.e.
332 Northern Ireland) and NE (i.e. Scotland) of the NE Irish Rockall Basin (Fig. 1A). The abundant
333 volcanic glass, which is indicative of magma-water interaction (e.g. Friedman & Long, 1984),
334 and tuffaceous material may have been derived from relatively proximal, offshore volcanic
335 sources, such as submarine volcanoes or hydrothermal vents genetically related to the
336 underlying sill-complex. However, the fact the glass is weathered argues against this
337 interpretation. The clay-rich nature of these sandstones likely reflects diagenetic degradation of
338 the mafic volcanic grains forming the bulk of the depositional unit (cf. Primmer et al, 1997).

339 In contrast to the volcanic terrain-derived sandstones, the quartzose-feldspathic
340 sandstones at the base of upper Paleocene (Pal. 2) were more likely derived from a sedimentary
341 or meta-sedimentary source area. We can interpret the compositional differences between the
342 upper (Pal. 1) and lower (Pal. 2) sandstones in one of two ways: (i) the sandstones were sourced
343 from different locations; i.e. the majority of the sandstones were derived from a regionally
344 extensive, volcanic source area (Pal. 1), whereas the oldest, quartzose-feldspathic sandstones
345 at the base of Pal. 2 were derived from a more local, sedimentary or meta-sedimentary source
346 area; or (ii) the amount of contemporaneous volcanism changed through time; i.e. the basal,
347 quartzose-feldspathic sandstones near the base of Pal. 2 were deposited prior to emplacement
348 of the widespread volcanic terrain that now dominates the northern basin margin, whereas
349 younger sandstones (i.e. most of Pal. 2 and all of Pal. 1) were deposited later, either synchronous
350 with and/or after widespread volcanism.

351 The upper Paleocene succession encountered in 12/2-1 (Dooish) is markedly different
352 to that in 5/22-1. First, quartzose-feldspathic sandstones, broadly similar in composition to
353 those near the *base* of 5/22-1, are instead found near the *top* of the upper Paleocene succession
354 in 12/2-1. Second, volcanoclastic sandstones are also present in 12/2-1, but they occur near the
355 base rather than near the top of the upper Paleocene succession (cf. 5/22-1; Fig. 4). The reason
356 for this variability is unclear, although it might point to temporal and spatial changes in the
357 provenance of the Paleocene deep-water sandstones, with time-equivalent sands being sourced
358 from either a meta-sedimentary or a volcanic source area (see discussion above). However, due
359 to a lack of biostratigraphic data we are unable to directly correlate upper Paleocene sandstones
360 between 5/22-1 and 12/2-1, and because the sandstones are relatively thin (<5 m) we are unable
361 to directly map them in seismic reflection data. Nonetheless, seismic data clearly indicate that
362 the entire Paleocene interval thins across the Errigal forced fold (see Magee et al., 2014),
363 suggesting the structure grew during this time and may have influenced reservoir deposition
364 (see discussion below) (Smallwood & Maresh, 2002; Egbeni et al., 2014).

365

366 **THERMAL HISTORY**

367

368 Only traces of hydrocarbons are reported in 5/22-1, with the main upper Paleocene sandstone-
369 bearing intervals being water-bearing (Supplementary items 1 and 6). However, dead oil was
370 noted in cuttings from intervening siltstones, which, along with the nearby Dooish discovery,
371 clearly indicates the presence of a working petroleum system in the NE Irish Rockall Basin.
372 These observations imply that source rocks are present in the basin, and that the thermal history
373 of the basin led to maturation of these source rocks (see below). Given the basin's tectono-
374 stratigraphic development, its thermal history likely reflects: (i) regional (i.e. basin-scale)
375 heating due to rifting; (ii) regional cooling due to post-rift, intra-plate shortening and uplift,
376 likely related to plate break-up and associated ridge push (e.g. Tuitt et al., 2010), or magmatic
377 underplating (e.g. Brodie and White, 1994); and (iii) local heating driven by the emplacement
378 of igneous intrusions, some of which extend upwards into the reservoir-bearing Paleocene
379 succession (e.g. the sill located only c. 1.5 km to the NW of 5/22-1 in Fig. 2). It is likely that
380 rift-related heating drove source rock maturation of Carboniferous coals for Dooish, which,
381 although overlain by a single, 15 m thick intrusion, does not appear to be spatially related to a
382 very large intrusion complex, unlike Errigal (Fig. 2).

383 A key question is whether local, intrusion-induced heating was responsible for the poor
384 reservoir quality observed within the upper Paleocene succession in Errigal. More specifically,
385 did contact metamorphism and/or intrusion-induced fluid circulation result in the degradation
386 of volcanic grain assemblages, the clogging of pore space, blocking of pore throats and
387 therefore the overall poor reservoir quality? To try and answer this question we examine FIM,
388 VR and AFTA data obtained from sidewall core samples from the reservoir-bearing, Upper
389 Paleocene succession. These data could help us determine whether the reservoir-bearing
390 interval experienced elevated temperatures during burial in response to the emplacement of sills
391 in Upper Cretaceous-to-Paleocene mudstones (see methodology outlined in Supplementary
392 items 3 and 4; data from these Supplementary items are synthesized in Figs 7-9 and shown in
393 Tables 1 and 2).

394

395 **Fluid Inclusion Microthermometry and fluorescence petrography**

396

397 *Results.* Microthermometry and fluorescence petrography was performed on fluid inclusions
398 by the operator on samples from 12 sidewall cores taken from the Paleocene succession in 5/22-
399 1 (Fig. 7; see also Supplementary Item 3). Primary aqueous fluid inclusions were found in
400 analcime cement and authigenic quartz. The majority (91%; i.e. 31 of 34) of analcime-hosted
401 primary inclusions were monophasic, indicating formation below 60°C. However, some two-
402 phase inclusions (9%; i.e. 3 of 34) are present that exhibit higher homogenisation temperatures
403 of 108°C to 119°C. (Fig. 7). Homogenisation temperatures recorded in primary inclusions of

404 quartz overgrowths in the lowermost sandstones (3916 and 3925 m; Pal. 2) range from 66°C to
405 82°C. Salinity of all primary inclusions is brackish (1.1-2.3% NaCl equivalent) to low (0.1-
406 0.5% NaCl equivalent) for analcime and authigenic quartz, respectively.

407 One healed microfracture in a quartz grain contained petroleum- and associated water-
408 bearing fluid inclusions (3490 m; Figs 4 and 7). These inclusions record fluid precipitation and
409 trapping at higher temperatures (120-125°C) and salinities (3.4% NaCl equivalent) than that
410 observed in analcime and the authigenic quartz (Fig. 7; see also Supplementary Item 3).

411

412 *Interpretation.* Given that: (i) the present bottom hole temperature is 76°C; and (ii) based on
413 the assumption that the rocks are presently at or near their maximum burial depth, most
414 homogenisation temperatures indicate fluid trapping and/or resetting at temperatures consistent
415 with their present burial depth. However, some samples contain evidence for elevated
416 homogenisation temperatures, possibly related to a very brief period of localised hot fluid flow
417 (see Supplementary items 3 and 4; see also discussion below). The detrital grain-hosted quartz
418 microfracture at 3490 m also contains evidence for elevated paleotemperatures. However, the
419 related fluids are considerably more saline than that encountered in other primary inclusions,
420 suggesting they may not have been trapped *in situ*, but were rather ‘inherited’ from the grain
421 source area. As such, this sample may not record the burial-related history of the succession
422 penetrated by 5/22-1).

423

424 **Vitrinite Reflectance (VR)**

425

426 *Results.* VR was analysed for 26 cutting samples in 5/22-1. As discussed in Supplementary item
427 4, confidence levels for individual determinations are moderate to low. However, no significant
428 differences exist between the most and least reliable results. Despite low confidence levels and
429 scatter around the overall trend (see below), the results arising from the VR and AFTA analysis
430 are at least consistent, suggesting the former provides a reliable assessment of maturity levels
431 and the basin thermal history. VR values vary from 0.27% to 0.48%, corresponding to
432 temperatures of <50°C to 80°C (Fig. 8 and Table 1). Temperatures broadly increase with depth.
433 The maturity of all samples, except for the second shallowest sample at 0.27%, are higher than
434 the ‘baseline’, burial-related heating only, thermal history (red line in Fig. 8; see also
435 Supplementary item 4). In detail, anomalously high maturity levels are particularly apparent in
436 the 500 m thick, upper Paleocene-to-middle Eocene interval (between c. 3100-3600 m) that
437 contains the poor-quality, volcanoclastic reservoirs (Pal. 1) (Fig. 8; see also Fig. 4).

438

439 *Interpretation.* Temperatures broadly increase with depth; this is consistent overall with burial-
440 related heating (Fig. 8). However, the anomalously high maturity levels in the upper Paleocene-

441 to-middle Eocene interval between c. 3100-3600 m indicate a temperature differential of on
442 average, 20°C. Elevated temperatures may record a localized heating effect resulting from the
443 passage of hot fluids (see below), an interpretation that at least broadly supports that derived
444 from Fluid Inclusion Microthermometry and fluorescence petrography (see above).

445

446 **Apatite Fission Track Analysis (AFTA)**

447

448 *Results.* AFTA was performed on seven cutting samples in 5/22-1 (Supplementary item 4). In
449 general, the high apatite yields and analysis are deemed to be of very high quality, providing
450 reliable constraints on thermal history (Supplementary Item 4). However, apatites from all
451 samples contain a large proportion of fission tracks formed prior to deposition, an observation
452 that can impact the thermal history interpretation. One of the samples collected between 3575
453 and 3800 m had a mean track length of 1.4 μm shorter than predicted by the ‘baseline’ burial-
454 related heating only thermal history, whereas five out of the remaining seven samples had
455 lengths \sim 1.4-2 μm shorter than predicted. For one sample only two track lengths were
456 measured, and so cannot be used to assess its thermal history.

457

458 *Interpretation.* The occurrence of track lengths shorter than predicted by the ‘baseline’ burial-
459 related heating only thermal history can be explained by either an inherited signal from the
460 sediment source terrain, elevated paleotemperatures after deposition, or a combination of both.
461 If we interpret this signal was *not* inherited from the source terrain, these data suggest the onset
462 of cooling of the studied samples from paleotemperatures 15-45°C above the present, sometime
463 between 40 and 10 Ma. This interpretation would be consistent with the results arising from the
464 FIM and VR analyses presented above, which suggest a localised heating event in the Paleocene
465 succession, perhaps related to the passage of hot fluids. We also note that the oldest age for the
466 onset of cooling (c. 40 Ma; middle Eocene) post-dates the latest period of magmatism
467 constrained by Magee et al. (2014).

468

469 **DISCUSSION**

470

471 No significant oil shows were discovered in 5/22-1, although traces were reported at 3420 m
472 (lower Eocene), 3690 m (upper Paleocene) and 3900 m (lower Paleocene) (Supplementary Item
473 6). Headspace and cuttings gas data provide only weak evidence for relatively dry, thermogenic
474 gas in the Cretaceous-to-Paleocene succession (Supplementary Item 6). We here critically re-
475 evaluate why 5/22-1 failed, and examine the broader role breakup-related magmatism may play
476 in controlling the future prospectivity of the NE Irish Rockall Basin and other magmatically
477 influenced basins.

478

479 **Why did Errigal fail?**

480

481 *Source presence, maturation, and migration.* The Dooish gas discovery (12/2-1) provides
482 evidence for a working source rock in the NE Irish Rockall Basin. However, the type (e.g.
483 marine, non-marine, or mixed; Type I-III), richness (e.g. TOC), and distribution of, and the
484 stratigraphic level at which this source rock occurs (e.g. Carboniferous, Lower or Upper
485 Jurassic) remains highly uncertain. VR data from 5/22-1 indicate Cretaceous-to-Paleocene
486 mudstones are under mature, even for oil (i.e. they have VR values substantially <0.5%; see
487 Fig. 8), suggesting they were not the source for the gas in Dooish or the gas encountered in the
488 Cretaceous-to-Paleocene succession in 5/22-1. Thus, despite being heavily intruded, a process
489 which could locally mature otherwise regionally immature source rocks (e.g. Schutter, 2003;
490 Rodriguez Monreal et al., 2009; Aarnes et al., 2015; Muirhead et al., 2017), these mudstones
491 appear unable to generate appreciable volumes of hydrocarbons.

492 Given there is good evidence for the presence of mature source rock in the NE Irish
493 Rockall Basin, it is thus important to consider whether migration was reason Errigal failed.
494 Errigal is underlain by extensive sill-complex (Fig. 2). In addition to our 82 seismically
495 resolvable and mapped sills, it is likely that additional, sub-seismic sills, and possibly sub-
496 vertical (and thus poorly imaged) dykes are present. For example, based on seismic reflection
497 and borehole data from the Faroe-Shetland Basin, Schofield et al. (2015) argue that 88% of sills
498 may be sub-seismic (i.e. <40 m thick), leading to a drastic underestimation of the total volume
499 of sill-hosted igneous material. In the NE Irish Rockall Basin we cannot constrain the
500 permeability of individual sills or their host rock due to a lack of deep borehole data. We
501 therefore provide two hypotheses for the permeability structure of interval separating source
502 and reservoir rocks. First, the intrusions could be permeable due to the presence of cooling-
503 induced fractures (e.g. Rateau et al., 2013; Rodriguez Monreal et al., 2009; Senger et al., 2015;
504 Schofield et al., 2017; Mark et al., 2018). The host rock could also be permeable due to the
505 development of burial-related fracture networks, which may have been enhanced by
506 overpressure development and hydrofracture development (e.g. Cosgrove, 2004;
507 Gudmundsson, 2011). In this case, any gas (or oil) generated by the source rock could have
508 migrated relatively freely up into the shallower reservoirs. An alternative interpretation is that
509 the bulk permeability of the sub-reservoir sill-complex is relatively low (i.e. the sills and their
510 host rock are only weakly fractured). In this case, any hydrocarbons expelled from pre-
511 Cretaceous source rocks would have been unable to migrate into the Errigal trap due to the
512 baffling effects of the heavily intruded Cretaceous succession (cf. Schofield et al., 2018). These
513 hydrocarbons may have instead been diverted southwards, up structural dip, towards the fault-
514 block trap penetrated by 12/2-1 (Dooish), located only c. 42 km to the south (Fig. 2). A similar

515 scenario is envisaged for the prospects targeted by 164/25-1z, 164/27-1 (Antaeus) and 154/1-2
516 (Benbecula North) in the UK Rockall, and may be a more general risk for sill-induced forced
517 fold prospects (Schofield et al., 2018).

518

519 *Trap.* Borehole 5/22-1 targeted a c. 55 km² four-way dip-closure that formed a relatively small
520 part of a much larger (c. 224 km²), dome-shaped structure. This structure (a ‘forced fold’)
521 formed due to the forcible emplacement of an igneous sill-complex over a c. 15 Myr period in
522 the earliest Paleocene to early Eocene (Magee et al., 2014). The trap was well-imaged in seismic
523 data and was considered robust, with uncertainties in seismic velocities leading to modest
524 uncertainties in predicted trap size, column height, and depth to top reservoir.

525 Although 5/22-1 was unsuccessful, similar forced fold traps have been successfully
526 targeted in other volcanic basins. For example, the Tulipan discovery (6302/6-1), Møre Basin,
527 offshore mid-Norway discovered gas in lower Paleocene deep-water sandstones contained in
528 an early Eocene forced fold. In a similar manner to the structure targeted by 5/22-1, the Tulipan
529 fold formed in response to sill emplacement in Upper Cretaceous mudstone (Schmiedel et al.,
530 2017). Gas was also discovered in the Benbecula South prospect (154/1-1), UK Rockall. This
531 discovery is characterised by a Paleocene deep-water sandstone reservoir contained within a
532 well-defined four-way dip closure, representing a sill-induced forced fold (Schofield et al.,
533 2018). The Loanan prospect (214/23-1), Faroe-Shetland Basin, offshore UK again targeted
534 Paleocene deep-water sandstones incorporated in a sill-induced forced fold. Although the
535 results of the well are tight, the well did not reach the lower target or its target (total) depth
536 because of concerns related to the distribution and related pressure state of nearby sills (Mark
537 et al., 2018).

538 Further afield, the Wichian Buri oil field, Phetchabun Basin, Thailand is an excellent
539 example of a hydrocarbon accumulation associated with the emplacement of igneous rocks. In
540 this location, emplacement of a dolerite laccolith caused forced folding of a lacustrine-fluvial
541 clastic succession and the formation of a large trap (Schutter, 2003 and references therein).
542 Borehole Perindi-1, NW Canning Basin, offshore NW Australia targeted one of several,
543 relatively small (3-16 km² in areal extent; vertical closures of up to 120 m) forced folds
544 developed above Permian saucer-shaped sills (Reeckmann and Mebberson, 1984). Although
545 the well penetrated thick (i.e. several hundred metres), high-quality (>25% porosity) sandstone
546 reservoirs, capped by a thick (50-90 m) mudstone seal, the borehole was water-wet. However,
547 the presence of oil shows indicates a working petroleum system, suggesting hydrocarbons
548 migrated into and out of the structure. Reeckmann and Mebberson (1984) speculate Perindi-1
549 failed due to breaching of the seal by and loss of hydrocarbons along numerous normal faults
550 developed at the dome crest. Because they are spatially restricted to the dome crest and because
551 they die-out downwards, we infer that these faults formed due to outer-arc stretching of the fold

552 during sill emplacement (cf. Hansen and Cartwright, 2006; Magee et al., 2013a; Magee et al.,
553 2017). Sill emplacement may, therefore, drive growth of relatively large and therefore attractive
554 forced fold-related traps, although a key risk is seal breach by outer-arc stretching-related
555 normal faults.

556

557 *Reservoir.* Upper Paleocene volcanoclastic deep-water sandstones are generally clay-rich and
558 of poor-quality (Pal. 1), likely due reflecting diagenetic degradation of the abundant volcanic
559 grains forming the bulk of the primary depositional unit. In this sense, the poor reservoir quality
560 is provenance related. Paleothermometric data from 5/22-1 suggest that, at some point in the
561 past and to varying degrees, the reservoir-bearing upper Paleocene interval experienced
562 temperatures higher than present. This heating may have enhanced and/or accelerated
563 diagenetic degradation of the volcanic grains, yielded clay minerals, and essentially made a bad
564 reservoir worse. We suggest this heating was caused by hot fluid circulation triggered by the
565 emplacement of nearby intrusive bodies, such as the large (i.e. seismically imaged) sill located
566 only c. 1.5 km NW of 5/22-1 (Fig. 2). The presence of low-salinity inclusions suggest input of
567 low-salinity meteoric fluids derived from deeper strata, or potentially from metamorphic fluids
568 (Yardley & Graham, 2002) expelled from sill intrusions.

569 It is also possible that the elevated temperatures could simply reflect elevated heat flow
570 accompanying a late-Cenozoic to Palaeogene phase of rifting that affected the Faroe-Shetland
571 Basin, an event that could have extended southwards into the NE Irish Rockall Basin
572 (Scotchman et al., 2006). However, this model does not explain why ‘normal’ (i.e. consistent
573 with that predicted by paleothermal modelling) temperatures are encountered at deeper depths,
574 in Upper Cretaceous strata at the base of 5/22-1 (Fig. 8). It is important to note that thin intervals
575 of good-quality reservoir do occur at the base of the succession (Pal. 2; Fig. 4), suggesting
576 Errigal did not fail due to lack of reservoir, but possibly charge (see above). Reservoir quality
577 does however remain a concern for the NE Irish Rockall, the broader NE Atlantic Margin, and
578 magmatically influenced basins in general.

579 Rather than documenting sill- or rift-induced, elevated temperatures in upper
580 Paleocene-to-upper Eocene samples may instead record hydrothermal venting of heated fluids
581 and host sediment onto the seafloor via sill-fed vents. These fluids and sediment would have
582 been sourced from the intruded Upper Cretaceous succession. This process is inferred to have
583 led to mixing and thermal maturation of sediments vented around the Tulipan Sill, Møre Basin,
584 offshore mid-Norway (Hafeez et al., 2017; Kjoberg et al., 2017). We see some evidence for
585 Eocene extrusive activity, yet the products of this lie several hundred metres above the interval
586 in which elevated paleotemperatures are observed (Figs 2 and 8; see also Fig. 11 in Magee et
587 al., 2014).

588

589 *Seal*. As we discussed above, intrusion-induced forced folds can be deformed by coeval normal
590 faults (Hansen & Cartwright, 2006; Magee et al., 2013a; 2017), which may facilitate vertical
591 leakage of hydrocarbons from otherwise valid traps (Reeckmann & Mebberson, 1984). Our
592 seismic data present only very limited evidence for the widespread development of seismic-
593 scale normal faults across the Errigal dome (Fig. 2). This implies outer-arc stretching-induced
594 normal faulting probably did not cause the Errigal borehole to fail. Our interpretation is
595 supported by the observation that one tentative hydrocarbon show was detected within the
596 Errigal structure, implying hydrocarbons did not migrate into and then out of the trap (cf.
597 Reeckmann & Mebberson, 1984).

598

599 **How might breakup-related magmatism influence future prospectivity in the NE Irish** 600 **Rockall Basin?**

601

602 Breakup-related magmatism in the NE Irish Rockall Basin appears to have positively and
603 negatively impacted on petroleum system development in this frontier basin. For example,
604 emplacement of the igneous sill-complex drove the formation of a dome-shaped forced fold,
605 which represents a large, attractive, four-way dip closure incorporating pre-kinematic reservoirs
606 (Fig. 5A). Intrusions, if fractured, may have also facilitated hydrocarbon migration through
607 otherwise sealing, Cretaceous mudstone-dominated sequences, from deeply Palaeozoic and
608 Mesozoic source rocks to Paleocene reservoirs (e.g. Rateau et al., 2013; Mark et al., 2017).
609 However, the spatially extensive sill-complex (Fig. 2), if poorly fractured, may have had bulk
610 low permeability and thus impeded or deflected laterally the otherwise vertical migration of
611 pre-Cretaceous-sourced hydrocarbons, if generated (e.g. Thomaz Filho et al., 2008; Schofield
612 et al., 2018). Sills may also act as reservoirs, with hydrocarbons hosted in cooling-related
613 fractures. Such reservoirs can be significant, with estimated recoverable reserves thought to be
614 c. 30 million barrels (MMbbl) in the Wichian Buri oil field, Phetchabun Basin, Thailand
615 (Schutter, 2003). Although seemingly not the case in this part of the NE Irish Rockall Basin,
616 local intrusion-induced heating could have triggered maturation and gas expulsion from even
617 organically poor Cretaceous mudstones underlying the prospective Paleocene level, or
618 preserved in deep rift basins adjacent to structurally high fault blocks. Such a process is thought
619 to have triggered maturation of organically poor (i.e. 1% wt organic carbon) Cretaceous
620 mudstones on the Utgard High, offshore Norway (Aarnes et al., 2015).

621 Although Errigal failed, data collected during drilling are very useful, indicating
622 reservoir-quality deep-water sandstones were at least locally deposited in the region during the
623 Late Paleocene and Eocene, and that the upper Paleocene, reservoir-bearing succession is
624 capped by a thick, post-Eocene seal (Figs 1C and 4). As such, we consider that the post-

625 Cretaceous succession of the NE Irish Rockall Basin remains prospective. For example,
626 although the intrusion-induced structural trap failed, additional prospectivity may remain in
627 stratigraphic traps on the forced fold limbs. Intrusion-induced forced folding can drive syn-
628 depositional deformation of the seabed, causing deflection and controlling the routing of
629 sediment gravity-currents (Smallwood and Maresh, 2002; Egbeni et al., 2014). Turbidites may
630 thin and onlap towards, and thus be absent at, the fold crest, a stratigraphic architecture that
631 provides the opportunity for development of stratigraphic traps. Charging such traps remains
632 challenging due to the presence of the underlying, largely impermeable sill-complex, which
633 may act to divert ascending hydrocarbons away from overlying traps.

634

635 **CONCLUSIONS**

636

637 We use 3D seismic reflection, borehole, petrographic, and paleothermometric data to document
638 the geology of borehole 5/22-1 (the Errigal prospect), NE Irish Rockall Basin, offshore western
639 Ireland. We conclude that:

640

- 641 1. Errigal tested a large (55 km²) four-way dip closure that formed to accommodate
642 emplacement of a Paleocene-to-Eocene igneous sill-complex.
- 643 2. Two water-bearing turbidite sandstone-bearing intervals occur in the Upper Paleocene
644 target interval of interest; the lowermost interval is low net-to-gross (c. 3%) and
645 contains thin (c. 5 m), quartzose-feldspathic sandstones of good reservoir quality (up
646 to 16%), whereas the upper interval is also of low net-to-gross (<1%), but in contrast
647 is dominated by thin (1-4 m), very poor-quality volcanoclastic sandstones.
- 648 3. The poor reservoir quality also likely reflects the primary composition of the reservoir,
649 which is dominated by volcanic grains and related clays derived from an igneous rock-
650 dominated, sediment source area.
- 651 4. Paleothermometric data (FIM, VR, AFTA) provide evidence for anomalously high
652 temperatures in the Paleocene-to-Eocene succession, suggesting that the poor reservoir
653 quality may also reflect sill-induced heating, fluid flow, and related diagenesis (i.e.
654 degradation of volcanic glass to pore-filling and pore throat-clogging clay minerals).
- 655 5. Errigal appeared to fail due to a lack of hydrocarbon charge; i.e. the low bulk
656 permeability of the heavily intruded Cretaceous mudstone succession may have
657 impeded vertical migration of sub-Cretaceous-sourced hydrocarbons into supra-
658 Cretaceous reservoirs.
- 659 6. Breakup-related magmatism in the NE Irish Rockall Basin positively and negatively
660 impacted the petroleum system development in this frontier basin. For example, sill-
661 complex emplacement drove formation of a large trap, whereas these low-permeability

662 sills may have been the reason hydrocarbons were unable to migrate and charge supra-
663 sill reservoirs.

664 7. Exploration potential remains in the NE Irish Rockall Basin, with future targets
665 includes stratigraphically trapped, Paleocene-to-Eocene deep-water sandstones
666 onlapping the flanks of intrusion-induced forced folds, structurally trapped, intra-
667 Cretaceous deep-water sandstones incorporated within intrusion-induced forced folds,
668 and more conventional, Mesozoic fault-block traps underlying the heavily intruded
669 Cretaceous succession (e.g. Dooish).

670

671 **ACKNOWLEDGEMENTS**

672

673 The Department of Communications, Energy and Natural Resources (Petroleum Affairs
674 Division), Ireland, is thanked for providing seismic and borehole data. Individuals and
675 contractor companies who undertook the primary analysis of FIM, AFTA and VR data, as well
676 as compiled the composite logs and final well reports, are also thanked; they are all mentioned
677 by name in the reports and data contained in the various Supplementary Items.

678

679 **DATA AVAILABILITY STATEMENT**

680

681 The seismic and borehole datasets analysed as part of this paper are available upon request IHS
682 Markit (releaseddata@ihs.com) (see also: [https://www.dccae.gov.ie/en-ie/natural-
683 resources/topics/Oil-Gas-Exploration-Production/data/Pages/Data.aspx](https://www.dccae.gov.ie/en-ie/natural-resources/topics/Oil-Gas-Exploration-Production/data/Pages/Data.aspx)).

684

685 **REFERENCES**

686

687 Allen, P.A. & Allen, J.R. (2013) Basin analysis: Principles and application to petroleum play
688 assessment. John Wiley & Sons.

689

690 Archer, S.G., Bergman, S.C., Iliffe, J., Murphy, C.M. & Thornton, M. (2005) Palaeogene
691 igneous rocks reveal new insights into the geodynamic evolution and petroleum potential of the
692 Rockall Trough, NE Atlantic Margin: Basin Research, 17, 171-201.

693

694 Aarnes, I., Planke, S., Trulsvik, M. & Svensen, H. (2015) Contact metamorphism and
695 thermogenic gas generation in the Vøring and Møre basins, offshore Norway, during the
696 Paleocene–Eocene thermal maximum. Journal of the Geological Society, 172, 588-598.

697

698 Berger, A., Gier, S. & Krois, P. (2009) Porosity-preserving chlorite cements in shallow-marine
699 volcanoclastic sandstones: Evidence from Cretaceous sandstones of the Sawan gas field,
700 Pakistan. AAPG Bulletin, 93, 595-615.
701

702 Bischoff, A.P., Nicol, A. & Beggs, M. (2017) Stratigraphy of architectural elements in a buried
703 volcanic system and implications for hydrocarbon exploration. Interpretation, 5, SK141-
704 SK159.
705

706 Brodie, J. & White, N.J. (1994) Sedimentary basin inversion caused by igneous underplating:
707 Northwest European continental shelf. Geology, 22, 147–150.
708

709 Broglia, C. & Ellis, D. (1990) Effect of alteration, formation absorption, and standoff on the
710 response of the thermal neutron porosity log in gabbros and basalts: Examples from Deep Sea
711 Drilling Project-Ocean Drilling Program Site. Journal of Geophysical Research, 95, 9171-9188.
712

713 Cosgrove, J.W. (2004) Hydraulic fracturing during the formation and deformation of a basin:
714 A factor in the dewatering of low-permeability sediments. AAPG Bulletin, 85, 737-748.
715

716 Delpino, D.H. & Bermúdez, A.M. (2009) Petroleum systems including unconventional
717 reservoirs in intrusive igneous rocks (sills and laccoliths). The Leading Edge, 28, 804-811.
718

719 Doré, A.G., Lundin, E.R., Jensen, L.N., Birkeland, Ø., Eliassen, P.E. & Fichler, C. (1999)
720 Principal tectonic events in the evolution of the northwest European Atlantic margin: Petroleum
721 Geology of Northwest Europe: Proceedings of the 5th Conference, 41-61.
722

723 Egbeni, S., McClay, K., Fu, J.J.K., & Bruce, D. (2014). Influence of igneous sills on Paleocene
724 turbidite deposition in the Faroe–Shetland Basin: a case study in Flett and Muckle sub-basin
725 and its implication for hydrocarbon exploration: Geological Society, London, Special
726 Publications, 397, 33-57.
727

728 Eide, C.H., Schofield, N., Jerram, D.A., & Howell, J.A. (2017) Basin-scale architecture of
729 deeply emplaced sill complexes: Jameson Land, East Greenland. Journal of the Geological
730 Society of London, 174, 23-40.
731

732 Emeleus, C.H. & Bell, B.R. (2005) British Regional Geology: the Palaeogene volcanic districts
733 of Scotland, 4th edn. British Geological Survey, Nottingham.
734

735 Farooqui, M.Y., Hou, H., Li, G., Machin, N., Neville, T., Pal, A., Shrivastva, C., Wang, Y.,
736 Yang, F., Yin, C. & Zhao, J. (2009) Evaluating volcanic reservoirs. *Oilfield Review*, 21, 36-
737 47.

738

739 Fernandes, K. (2011) Irish sills of the North Atlantic Igneous Province: seismic imaging,
740 observations and implications for climate change. Unpublished Ph.D Thesis. University of
741 Dublin, Trinity College, Dublin.

742

743 Friedman, I. & Long, W. (1984) Volcanic glasses, their origins and alteration processes.
744 *Journal of Non-Crystalline Solids*, 67, 127-133.

745

746 Grove, C., Jerram, D.A., Gluyas, J.G. & Brown, R.J. (2017) Sandstone diagenesis in sediment-
747 lava sequences: exceptional examples of volcanically driven diagenetic compartmentalization
748 in Dune Valley, Huab Outliers, NW Namibia: *Journal of Sedimentary Research*, 87, 1314-1335.

749

750 Gu, L.X., Ren, Z.W., Wu, C.Z., Zhao, M. & Qiu, J. (2002) Subvolcanic trachyte porphyry at
751 Oulituozi in the Liaohe basin and its mechanism for hydrocarbon reservoir formation. *AAPG*
752 *Bulletin*, 86, 1821-1832.

753

754 Gudmundsson, A. (2011). *Rock Fractures in Geological Processes*. Cambridge, UK:
755 Cambridge University Press. doi: 10.1017/CBO9780511975684.

756

757 Hafeez, A., Planke, S., Jerram, D.A., Millett, J.M., Maharjan, D. & Prestvik, T. (2017) upper
758 Paleocene ultramafic igneous rocks offshore mid-Norway: Reinterpretation of the Vestbrona
759 Formation as a sill complex. *Interpretation*, 5, SK103-SK120.

760

761 Hansen, D.M. (2006) The morphology of intrusion-related vent structures and their
762 implications for constraining the timing of intrusive events along the NE Atlantic margin:
763 *Journal of the Geological Society of London*, 163, 789-800.

764

765 Hansen, D.M., & Cartwright, J. (2006) The three-dimensional geometry and growth of forced
766 folds above saucer-shaped igneous sills: *Journal of Structural Geology*, 28, 1520-1535.

767

768 Hansen, J., Jerram, D.A., McCaffrey, K. & Passey, S.R. (2009) The onset of the North Atlantic
769 Igneous Province in a rifting perspective: *Geological Magazine*, 146, 309-325.

770

771 Haughton, P., Praeg, D., Shannon, P., Harrington, G., Higgs, K., Amy, L., Tyrrell, S. &
772 Morrissey, T. (2005) First results from shallow stratigraphic boreholes on the eastern flank of
773 the Rockall Basin, offshore western Ireland: Geological Society, London, Petroleum Geology
774 Conference series, 6, 1077-1094.
775

776 Hole, M.J. & Millett, J.M. (2016) Controls of mantle potential temperature and lithospheric
777 thickness on magmatism in the North Atlantic Igneous Province: *Journal of Petrology*, 57,
778 pp.417-436.
779

780 Holford, S.P., Schofield, N., Jackson, C.A-L., Magee, C., Green, P.F. & Duddy, I.R. (2013).
781 Impacts of igneous intrusions on source reservoir potential in prospective sedimentary basins
782 along the western Australian continental margin. *Proceedings of the Western Australia Basin*
783 *Symposium*.
784

785 Iyer, K., Schmid, D.W., Planke, S. & Millett, J. (2017) Modelling hydrothermal venting in
786 volcanic sedimentary basins: Impact on hydrocarbon maturation and paleoclimate. *Earth and*
787 *Planetary Science Letters*, 467, 30-42.
788

789 Jacquemyn, C., El Desouky, H., Hunt, D., Casini, G. & Swennen, R. (2014) Dolomitization of
790 the Latemar platform: Fluid flow and dolomite evolution: *Marine and Petroleum Geology*, 55,
791 43-67.
792

793 Jerram, D.A. & Widdowson, M. (2005) The anatomy of Continental Flood Basalt Provinces:
794 geological constraints on the processes and products of flood volcanism. *Lithos*, 79, 385-405.
795

796 Kjoberg, S., Schmiedel, T., Planke, S., Svensen, H.H., Millett, J.M., Jerram, D.A., Galland, O.,
797 Lecomte, I., Schofield, N., Haug, Ø.T. & Helsem, A. (2017) 3D structure and formation of
798 hydrothermal vent complexes at the Paleocene-Eocene transition, the Møre Basin, mid-
799 Norwegian margin. *Interpretation*, 5, SK65-SK81.
800

801 Magee, C., Briggs, F. & Jackson C.A-L. (2013a) Lithological controls on igneous intrusion-
802 induced ground deformation: *Journal of the Geological Society of London*, 170, 853-856.
803

804 Magee, C, Jackson, CA-L. & Schofield, N. (2013b) The influence of normal fault geometry on
805 igneous sill emplacement and morphology: *Geology*, 41, 407-410.
806

807 Magee, C., Jackson, C.A-L. & Schofield, N. (2014) Diachronous sub-volcanic intrusion along
808 deep-water margins: Insights from the NE Irish Rockall Basin: *Basin Research*, 26, 85-105.
809

810 Magee, C., Jackson, C.A-L., Hardman, J.P., & Reeve, M.T. (2017) Decoding sill emplacement
811 and forced fold growth in the Exmouth Sub-basin, offshore northwest Australia: Implications
812 for hydrocarbon exploration: *Interpretation*, 5, SK11-SK22.
813

814 Magee, C., Hoggett, M., Jackson, C.A-L., & Jones, S. (2019) Burial-related Compaction
815 Modifies Intrusion-induced Forced Folds: Implications for Reconciling Roof Uplift
816 Mechanisms using Seismic Reflection Data: *Frontiers in Earth Science*, 7, p39.
817

818 Mark, N.J., Schofield, N., Pugliese, S., Watson, D., Holford, S., Muirhead, D., Brown, R. &
819 Healy, D. (2018) Igneous intrusions in the Faroe Shetland basin and their implications for
820 hydrocarbon exploration; new insights from well and seismic data: *Marine and Petroleum*
821 *Geology*, 92, 733-753.
822

823 McClay, K., Scarselli, N. & Jitmahantakul, S. (2013) Igneous intrusions in the Carnarvon Basin,
824 NW Shelf, Australia: The sedimentary basins of Western Australia IV: Proceedings of the
825 Petroleum Exploration Society of Australia Symposium, Petroleum Exploration Society of
826 Australia, 1–20.
827

828 McKinley, J.M., Worden, R.H. & Ruffell, A.H. (2003) Smectite in Sandstones: A Review of
829 the Controls on Occurrence and Behaviour During Diagenesis: *Clay Mineral Cements in*
830 *Sandstones*, edited, pp. 109-128, Blackwell Publishing Ltd.
831

832 Millett, J.M., Wilkins, A.D., Campbell, E., Hole, M.J., Taylor, R.A., Healy, D., Jerram, D.A.,
833 Jolley, D.W., Planke, S., Archer, S.G. & Blischke, A. (2016) The geology of offshore drilling
834 through basalt sequences: Understanding operational complications to improve efficiency.
835 *Marine and Petroleum Geology*, 77, 1177-1192.
836

837 Muirhead, D.K., Bowden, S.A., Parnell, J. & Schofield, N. (2017) Source rock maturation
838 owing to igneous intrusion in rifted margin petroleum systems. *Journal of the Geological*
839 *Society*, 174, 979-987.
840

841 Naylor, D. & Shannon, P.M. (2005) The structural framework of the Irish Atlantic Margin. In
842 *Petroleum geology: N.W. Europe and Global Perspectives*, Proceedings of the 6th Petroleum
843 *Geology Conference.*, 1009-1021.

844

845 Primmer, T.J., Cade, C.A., Evans, J., Gluyas, J.G., Hopkins, M.S., Oxtoby, N.H., Smalley, P.C.,
846 Warren, E.A. & Worden, R.H. (1997) Global patterns in sandstone diagenesis: their application
847 to reservoir quality prediction for petroleum exploration: Reservoir quality prediction in
848 sandstones and carbonates, AAPG Memoir, 69, 61-77.

849

850 Rateau, R., Schofield, N. & Smith, M. (2013) The potential role of igneous intrusions on
851 hydrocarbon migration, West of Shetland: Petroleum Geoscience, 19, 259–272,

852

853 Reeckman, S.A. & Mebberson, A.J. (1984) Igneous intrusions in the north-west Canning Basin
854 and their impact on oil exploration: Proceedings of the Canning Basin Symposium, Perth:
855 Petroleum Exploration Society of Australia Ltd., 45–52.

856

857 Rodriguez Monreal, F., Villar, H.J., Baudino, R., Delpino, D. & Zencich, S. (2009) Modeling
858 an atypical petroleum system: a case study of hydrocarbon generation, migration and
859 accumulation related to igneous intrusions in the Neuquén Basin, Argentina: Marine and
860 Petroleum Geology, 26, 590-605.

861

862 Rohrman, M. (2007) Prospectivity of volcanic basins: trap delineation and acreage de-risking:
863 AAPG Bulletin, 91, 915–939.

864

865 Rohrman, M. (2015). Delineating the Exmouth mantle plume (NW Australia) from denudation
866 and magmatic addition estimates: Lithosphere, 7, 589-600.

867

868 Schmiedel, T., Kjoberg, S., Planke, S., Magee, C., Galland, O., Schofield, N., Jackson, C.A.L.
869 and Jerram, D.A., 2017. Mechanisms of overburden deformation associated with the
870 emplacement of the Tulipan sill, mid-Norwegian margin: Interpretation 5, SK23-SK38.

871

872 Schofield, N., Holford, S., Millett, J., Brown, D., Jolley, D., Passey, S.R., Muirhead, D., Grove,
873 C., Magee, C., Murray, J. & Hole, M. (2017) Regional magma plumbing and emplacement
874 mechanisms of the Faroe-Shetland Sill Complex: implications for magma transport and
875 petroleum systems within sedimentary basins: Basin Research, 29, 41-63.

876

877 Schutter, S.R. (2003) Hydrocarbon occurrence and exploration in and around igneous rocks:
878 Geological Society, London, Special Publications, 214, 7-33.

879

880 Senger, K., Buckley, S.J., Chevallier, L., Fagereng, Å., Galland, O., Kurz, T.H., Ogata, K.,
881 Planke, S. & Tveranger, J. (2015) Fracturing of doleritic intrusions and associated contact
882 zones: Implications for fluid flow in volcanic basins. *Journal of African Earth Sciences*, 102,
883 70-85.

884

885 Smallwood, J.R. & Maresh, J. (2002) The properties, morphology and distribution of igneous
886 sills: Modelling, borehole data and 3D seismic from the Faroe-Shetland area: Geological
887 Society, London, Special Publications, 197, 271–306.

888

889 Svensen, H., Planke, S., Malthe-Sørenssen, A., Jamtveit, B., Myklebust, R., Eidem, T.R. &
890 Rey, S.S. (2004) Release of methane from a volcanic basin as a mechanism for initial Eocene
891 global warming. *Nature*, 429, p.542.

892

893 Thomaz Filho, A., Mizusaki, A.M.P. & Antonioli, L. (2008) Magmatism and petroleum
894 exploration in the Brazilian Paleozoic basins. *Marine and Petroleum Geology*, 25, 143-151.

895

896 Thomson, K. & Hutton, D. (2004) Geometry and growth of sill complexes: insights using 3D
897 seismic from the North Rockall Trough. *Bulletin of Volcanology*, 66, 364-375.

898

899 Tuitt, A., Underhill, J.R., Ritchie, J.D., Johnson, H. & Hitchen, K. (2010) Timing, controls and
900 consequences of compression in the Rockall-Faroe area of the NE Atlantic Margin", *Petroleum*
901 *Geology: From Mature Basins to New Frontiers – Proceedings of the 7th Petroleum Geology*
902 *Conference*, B. A. Vining, S. C. Pickering.

903

904 Tyrrell, S., Souders, A.K., Haughton, P.D., Daly, J.S. & Shannon, P.M. (2010) Sedimentology,
905 sandstone provenance and palaeodrainage on the eastern Rockall Basin margin: evidence from
906 the Pb isotopic composition of detrital K-feldspar: Geological Society, London, *Petroleum*
907 *Geology Conference series*, 7, 937-952.

908

909 Wang, K., Chen, M., Ma, Y., Liu, K., Liu, L., Li, X. & Hu, W. (2012) Numerical modelling of
910 the hydrocarbon generation of Tertiary source rocks intruded by doleritic sills in the Zhanhua
911 depression, Bohai Bay Basin, China. *Basin Research*, 24, 234-247.

912

913 Wu, C., Gu, L., Zhang, Z., Ren, Z., Chen, Z. & Li, W. (2006) Formation mechanisms of
914 hydrocarbon reservoirs associated with volcanic and subvolcanic intrusive rocks: Examples in
915 Mesozoic–Cenozoic basins of eastern China. *AAPG Bulletin*, 90, 137-147.

916

917 Witte, J., Bonora, M., Carbone, C. & Oncken, O. (2012) Fracture evolution in oil-producing
918 sills of the Rio Grande Valley, northern Neuquén Basin, Argentina: AAPG Bulletin, 96, 1253-
919 1277.

920

921 Yardley, B.W.D. & Graham, J.T. (2002) The origins of salinity in metamorphic fluids:
922 *Geofluids*, 2, 249-256.

923

924 **Figure captions**

925

926 **Fig. 1.** (A) Location map of the Irish Rockall Basin (IRB) highlighting the distribution of
927 igneous intrusions and extrusions (offshore central complexes, red circles; onshore central
928 complexes and lavas, green ornament; offshore lavas, light grey ornament; seaward-dipping
929 reflectors, dark grey ornament; hydrothermal vents, black triangles) associated with the North
930 Atlantic Igneous Province (modified from Emeleus & Bell, 2005; Hansen, 2006). The
931 bathymetric contours (grey lines; spacing=500 m) delineate the boundaries of the Northern
932 Rockall Basin (NRB), Porcupine (PB), Hatton (HB), Faroe-Shetland (FSB), Møre (MB) and
933 Vøring (VB) basins, as well as the Hatton (H) and Rockall (R) banks, and the Vøring Plateau
934 (VP). The Anton-Dohrn Lineament Complex (ADLC) is also labelled. (B) Bathymetry map of
935 the Irish Rockall Basin, illustrating the location of the 3D seismic reflection survey and
936 positions of boreholes 12/2-1 (Dooish) and 5/22-1 (Errigal). Note the proximity of the study
937 area to the Hebridean Terrace Igneous Complex (HTIC). (C) Simplified chronostratigraphic
938 column for the interval of interest depicting the key lithologies identified in boreholes 12/2-1
939 and 5/22-1 (N.B. only for the depth interval 2250 m to borehole total depth or 'TD'), and our
940 seismic-stratigraphic framework (which extends from seabed down to the Permian). J=top
941 Jurassic; KI=intra-Lower Cretaceous; KC=top-Coniacian; K=top Cretaceous; P=top
942 Paleocene; E=top Lower Eocene (based on lithostratigraphic and chronostratigraphic data
943 provided in Supplementary items 1, 2 and 5; see also Magee et al., 2014). Proven or speculated
944 petroleum system elements are shown; So=source rock; R=reservoir rock; Se=seal rock.

945

946 **Fig. 2.** (A) Seismic section and (B) geoseismic section intersecting 12/2-1 (Dooish) and 5/22-
947 1 (Errigal), illustrating the overall geometry of the NE Irish Rockall Basin, and the seismic
948 expression, geometry and distribution of igneous sills. Note the low-relief dome penetrated by
949 5/22-1 and its spatial relationship to the underlying igneous sill-complex, which is largely
950 hosted in Upper Cretaceous rocks. Note also the lavas and a potential magmatic vent, both
951 located in Eocene strata (see Fig. 11 in Magee et al. 2014). Syn-rift III (Lower to Upper
952 Cretaceous) has a post-rift appearance in this section, onlapping onto the synrift I/II-cored fault
953 block drilled by 12/2-1; however, in other sections, this package thickens towards rift-related

954 normal faults and has a synrift character. See Fig. 1B for location. Vertical exaggeration (VE)
955 = *c.* x4. Legend for colours in (B) is shown in Fig. 1C.

956

957 **Fig. 3.** Interpreted seismic sections (left) and 3D time-structure maps (right) showing the
958 geometry of igneous sills in the NE Irish Rockall Basin. Numbers refer to sills described by
959 Magee et al. (2014); see Fig. 6c and d in Magee et al. (2014) for location of sills. White lines
960 on 3D time-structure maps show positions of the seismic sections.

961

962 **Fig. 4.** Simplified stratigraphic correlation between 12/2-1 (Dooish) and 5/22-1 (Errigal)
963 showing the principal lithologies encountered in the Upper Cretaceous to Lower Eocene
964 succession. Lithological interpretation is based largely on cuttings and sparse sidewall cores.
965 Pal. 1=informally defined stratigraphic unit 'Paleocene 1'; Pal. 2= informally defined
966 stratigraphic unit 'Paleocene 2'; see text for discussion and Supplementary Material Item 1 and
967 5 for additional details. Large coloured circles represent diagenetic features and small white-
968 grey circles represent the main petrographic rock types; see text for full discussion. Note that
969 two arkosic-lithic arenite samples (white) and two lithic arenite samples (light-grey) are closely
970 spaced and are thus represented by only one dot, hence the apparent sample number mismatch
971 with the QFL plot in Fig. 6. For location of boreholes see Figs 1B and 2.

972

973 **Fig. 5.** (A) Top Paleocene time-structure map (see Fig. 1C). Contour spacing = 50 m. Note the
974 location of 5/22-1 on the crest of a broad, low-relief dome. (B) Lower Eocene isochron (time-
975 thickness) map (see Fig. 1C). Note thinning of this succession across the broad, low-relief dome
976 defined at top Paleocene level (see (A)). (C) Map depicting the geometries and stacking pattern
977 of the 82, largely Upper Cretaceous-hosted igneous sills (see Figs 2 and 3). Note that sill
978 stacking density (and inferred bulk sill thickness) is greatest immediately below the broad, low-
979 relief dome identified at top Paleocene level (see (A)).

980

981 **Fig. 6.** (A) QFL (quartz-feldspar-lithics) derived from petrographic analysis of the Paleocene
982 succession in 5/22-1 (Errigal). Location of samples is shown in Fig. 4. Raw data is shown in
983 Supplementary Item 1. (B) Thin-section micrograph from sidewall core #38 (3587 m; upper
984 Paleocene). Note the dominance of volcanoclastic rock fragments (including volcanic glass; G),
985 the presence of subordinate quartz (Q) and feldspar (F), and the pore-filling analcite cement (a).
986 (C) Thin-section micrograph from sidewall core #18 (3916 m; upper Paleocene). Note the
987 dominance of detrital quartz (Q) and feldspar (F); volcanoclastic rock fragments v(G) are rare.
988 e=blue staining used to highlight pore space. See Supplementary Material Item 1 for additional
989 petrographic data.

990

991 **Fig. 7.** Plot showing fluid inclusion microthermometry data from 5/22-1 (Errigal). Note the
992 overall low homogenisation temperatures ($<90^{\circ}$) for all samples. See text for full discussion.
993 See Supplementary Material Item 3 for additional fluid inclusion-derived, microthermometric
994 data.

995

996 **Fig. 8.** Plot of VR vs. depth for 5/22-1 (Errigal). The degree of confidence in each vitrinite
997 reflectance value was provided by Enterprise Ireland, ranging from A (high) to E (low) (see
998 Supplementary Material 4 for discussion). No additional information was provided on what
999 constituted a high vs. low confidence value. Right-hand column shows simplified lithology (see
1000 Fig. 4). Error bars=one standard deviation; note that errors bars were not provided for two of
1001 the 'confidence level E' data points (red). See Supplementary Material Item 3 for additional
1002 details on paleothermal modelling parameters.

1003

1004 **Fig. 9.** (A) AFTA data (left) and present temperature (right) plotted against sample depth (and
1005 stratigraphic age). The dashed black line on the left-hand panel indicates the stratigraphic age
1006 of the penetrated succession. Note that in all cases, fission track ages are significantly higher
1007 than the respective stratigraphic ages, suggesting: (i) these apatites contain a large proportion
1008 of fission tracks formed prior to deposition of the host sediments; and (ii) post-depositional
1009 heating effects were modest. (B) Preferred thermal history interpretation of AFTA and VR data
1010 from 5/22-1 (Errigal). The origin of the cooling event at ca. 10 Ma is unknown, but could relate
1011 to regional basin uplift, the cause of which is also unknown. All data and interpretations are
1012 from Supplementary Item 4.

1013

1014 **Table 1.** Vitrinite reflectance (VR) and paleotemperature analysis interpretation of VR data
1015 from 5/22-1 (Errigal). 'Measured VR' values are mean reflectance values for each sample.
1016 Estimates of maximum paleotemperature were determined using an assumed heating rates of
1017 $1^{\circ}\text{C}/\text{Ma}$ and a cooling rate of $10^{\circ}\text{C}/\text{Ma}$.

1018

1019 **Table 2.** Apatite Fission Track Analysis (AFTA) data for 5/22-1 (Errigal). Note that present
1020 temperature estimates are based on an assumed mean seabed temperature of 5°C and a present-
1021 day thermal gradient of $26.5^{\circ}\text{C}/\text{km}$. Thermal history interpretation of AFTA data is based on
1022 an assumed heating rate of $1^{\circ}\text{C}/\text{Ma}$ and a cooling rate of $10^{\circ}\text{C}/\text{Ma}$. Quoted ranges for
1023 paleotemperature and onset of cooling correspond to $\pm 95\%$ confidence limits. See
1024 Supplementary Item 3 for additional details on paleothermal modelling parameters and
1025 uncertainties.

1026

1027 **Supplementary Item 1.** Well IRE 5/22-1 “Errigal Deepwater Exploration” Final Well Report.
1028 Volume 1: Geological and Petrophysical Evaluation. Republic of Ireland Continental Shelf Oil
1029 Well Records. Prepared by Toby Lenehan. Published in 2001. Report provided by the
1030 Petroleum Affairs Division (PAD). Curated by IHS Energy. Available for download from:
1031 [https://www.dccae.gov.ie/en-ie/natural-resources/topics/Oil-Gas-Exploration-](https://www.dccae.gov.ie/en-ie/natural-resources/topics/Oil-Gas-Exploration-Production/data/Pages/Data.aspx)
1032 [Production/data/Pages/Data.aspx](https://www.dccae.gov.ie/en-ie/natural-resources/topics/Oil-Gas-Exploration-Production/data/Pages/Data.aspx).

1033

1034 **Supplementary Item 2.** Wellsite litholog for ERRIGAL IRE 5/22-1. Wellsite geologists:
1035 James Hollands and Alastair Flood. Provided by the Petroleum Affairs Division (PAD).
1036 Available for download from: [https://www.dccae.gov.ie/en-ie/natural-resources/topics/Oil-](https://www.dccae.gov.ie/en-ie/natural-resources/topics/Oil-Gas-Exploration-Production/data/Pages/Data.aspx)
1037 [Gas-Exploration-Production/data/Pages/Data.aspx](https://www.dccae.gov.ie/en-ie/natural-resources/topics/Oil-Gas-Exploration-Production/data/Pages/Data.aspx).

1038

1039 **Supplementary Item 3.** Evidence for the conditions of cementation and petroleum
1040 emplacement from fluid inclusions, Eastern Rockall Basin, Eire. Republic of Ireland
1041 Continental Shelf Oil Well Records. Prepared by Fluid Inclusion Analyses (FIA). Report
1042 provided by the Petroleum Affairs Division (PAD). Curated by IHS Energy. Available for
1043 download from: [https://www.dccae.gov.ie/en-ie/natural-resources/topics/Oil-Gas-Exploration-](https://www.dccae.gov.ie/en-ie/natural-resources/topics/Oil-Gas-Exploration-Production/data/Pages/Data.aspx)
1044 [Production/data/Pages/Data.aspx](https://www.dccae.gov.ie/en-ie/natural-resources/topics/Oil-Gas-Exploration-Production/data/Pages/Data.aspx).

1045

1046 **Supplementary Item 4.** Thermal history reconstruction in Errigal deepwater exploration well
1047 5/22-1, using AFTA and vitrinite reflectance. Republic of Ireland Continental Shelf Oil Well
1048 Records. Published in 2001. Geotrack report #807. Prepared by P.F.Green (Geotrack). Report
1049 provided by the Petroleum Affairs Division (PAD). Curated by IHS Energy. Available for
1050 download from: [https://www.dccae.gov.ie/en-ie/natural-resources/topics/Oil-Gas-Exploration-](https://www.dccae.gov.ie/en-ie/natural-resources/topics/Oil-Gas-Exploration-Production/data/Pages/Data.aspx)
1051 [Production/data/Pages/Data.aspx](https://www.dccae.gov.ie/en-ie/natural-resources/topics/Oil-Gas-Exploration-Production/data/Pages/Data.aspx).

1052

1053 **Supplementary Item 5.** IRE 12/2-1 Dooish composite log. Wellsite geologists: Peter Geerlings
1054 and Nick O’Neill. Log compiled by Peter Geerlings and Toby Lenehan. Report provided by the
1055 Petroleum Affairs Division (PAD). Available for download from:
1056 [https://www.dccae.gov.ie/en-ie/natural-resources/topics/Oil-Gas-Exploration-](https://www.dccae.gov.ie/en-ie/natural-resources/topics/Oil-Gas-Exploration-Production/data/Pages/Data.aspx)
1057 [Production/data/Pages/Data.aspx](https://www.dccae.gov.ie/en-ie/natural-resources/topics/Oil-Gas-Exploration-Production/data/Pages/Data.aspx).

1058

1059 **Supplementary Item 6.** Geochemical report on well 5/22-1. Republic of Ireland Continental
1060 Shelf Oil Well Records. Published in 2001. Authored by Peter B. Hall (GeoLab Nor A/S).
1061 Report provided by the Petroleum Affairs Division (PAD). Curated by IHS Energy. Available
1062 for download from: [https://www.dccae.gov.ie/en-ie/natural-resources/topics/Oil-Gas-](https://www.dccae.gov.ie/en-ie/natural-resources/topics/Oil-Gas-Exploration-Production/data/Pages/Data.aspx)
1063 [Exploration-Production/data/Pages/Data.aspx](https://www.dccae.gov.ie/en-ie/natural-resources/topics/Oil-Gas-Exploration-Production/data/Pages/Data.aspx).

Fig. 1

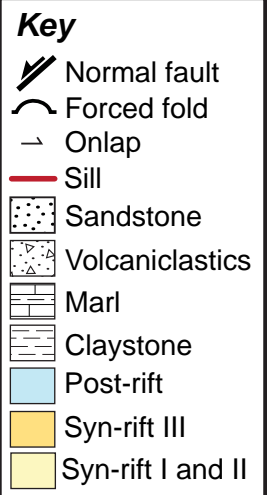
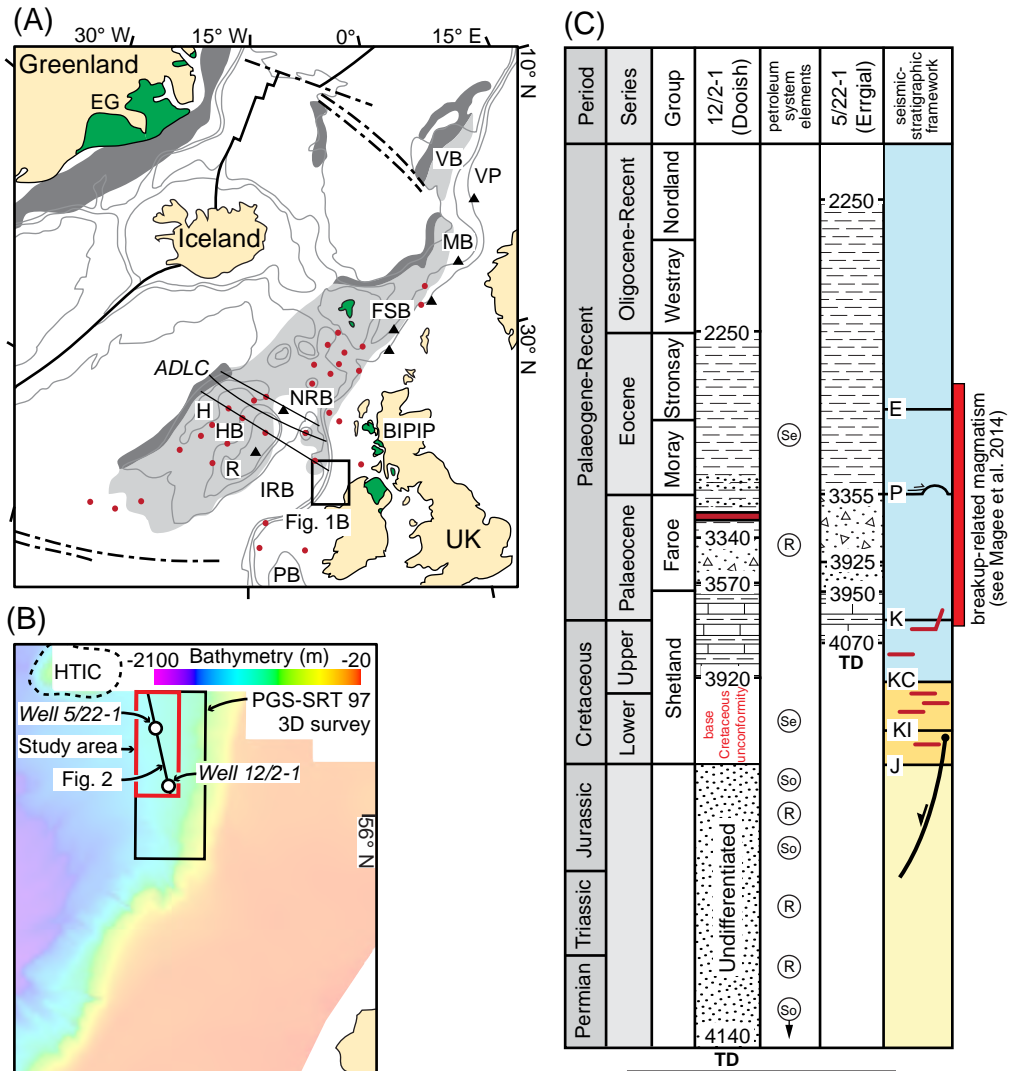


Fig. 2

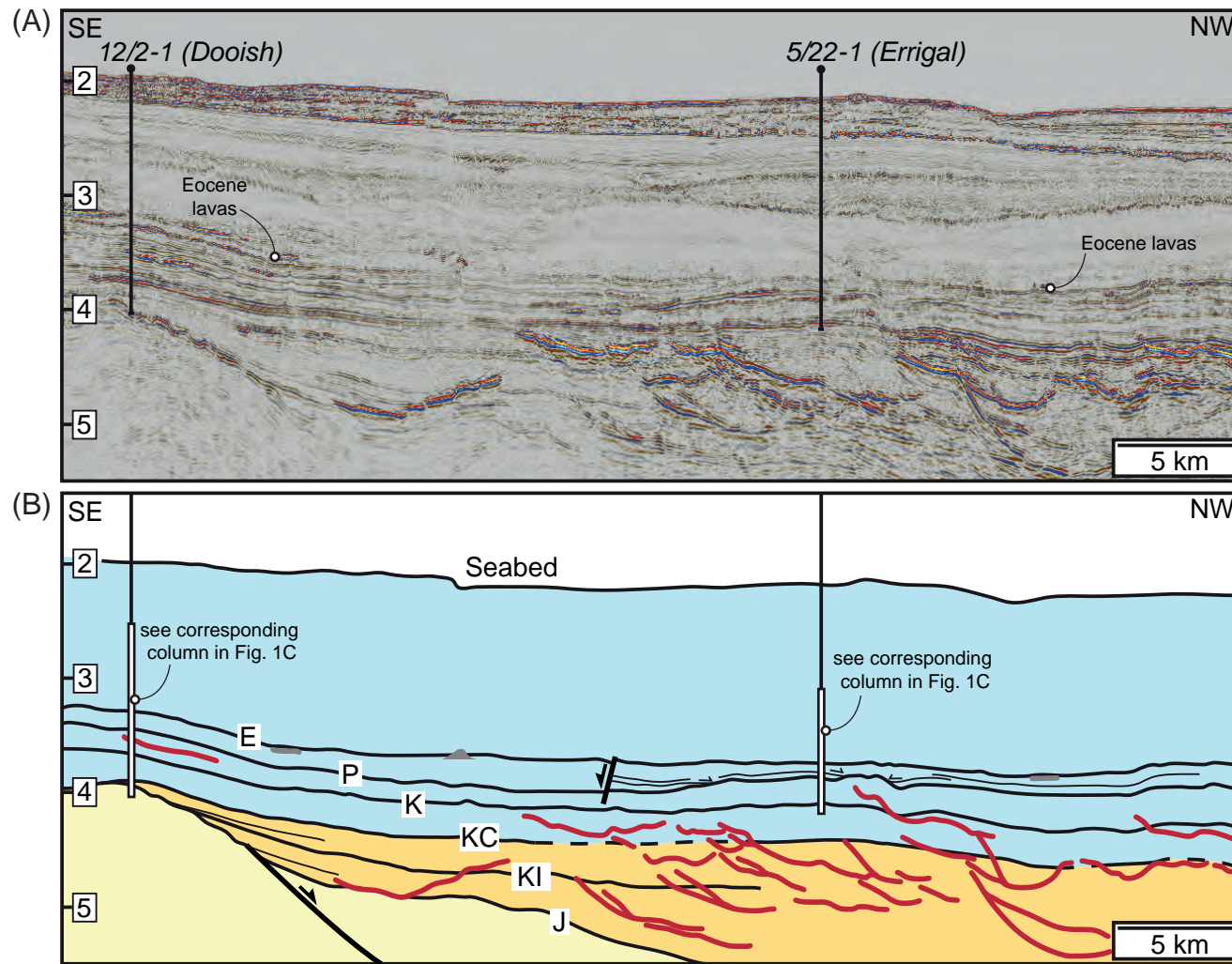


Fig. 3

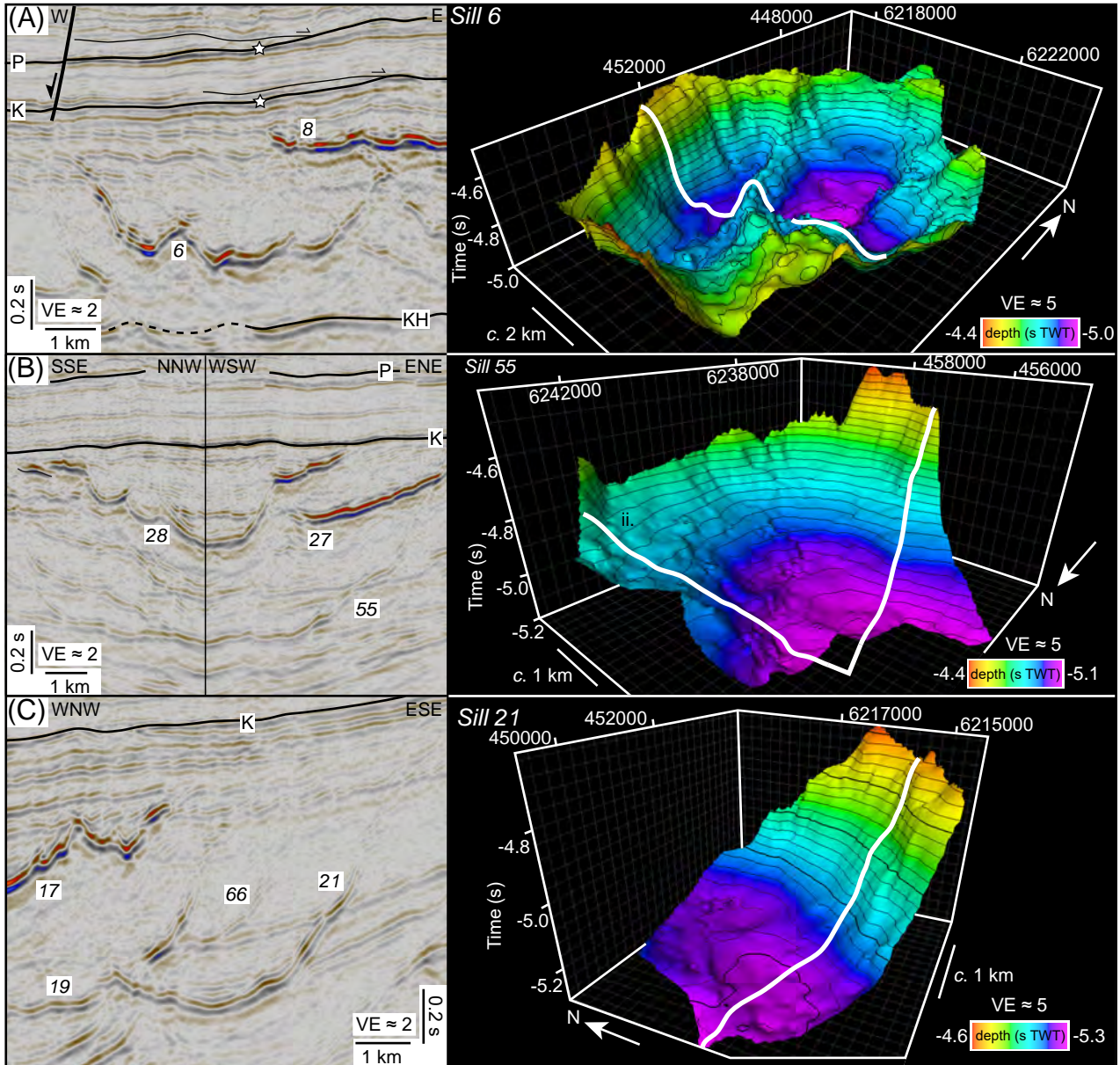
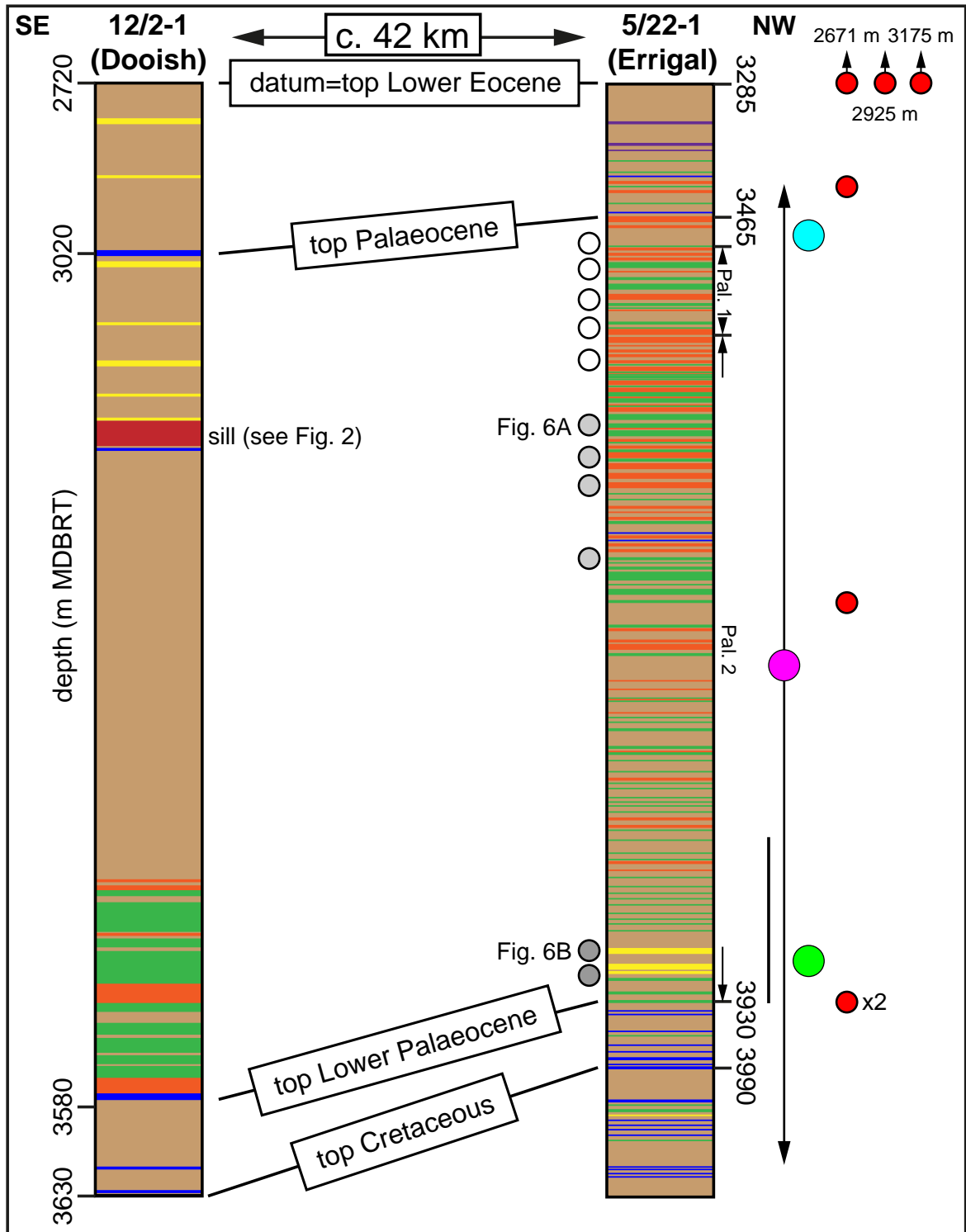


Fig. 4



Key

- | | | | |
|---------------------------------|--------------------------|---------------------------------|----------|
| mudstone | tuff (Balder Tuff Mbr) | arkosic-lithic arenites | } Fig. 6 |
| marl | volcaniclastic sandstone | lithic arenites | |
| siltstone | dolerite sill | sub-arkose | } Fig. 7 |
| quartzose-feldspathic sandstone | | analcite (3398-4070 m) | |
| | | quartz overgrowth (3916-3952 m) | |
| | | quartz microfracture (3490 m) | |
| | | AFTA samples (Fig. 9) | |

Fig. 5

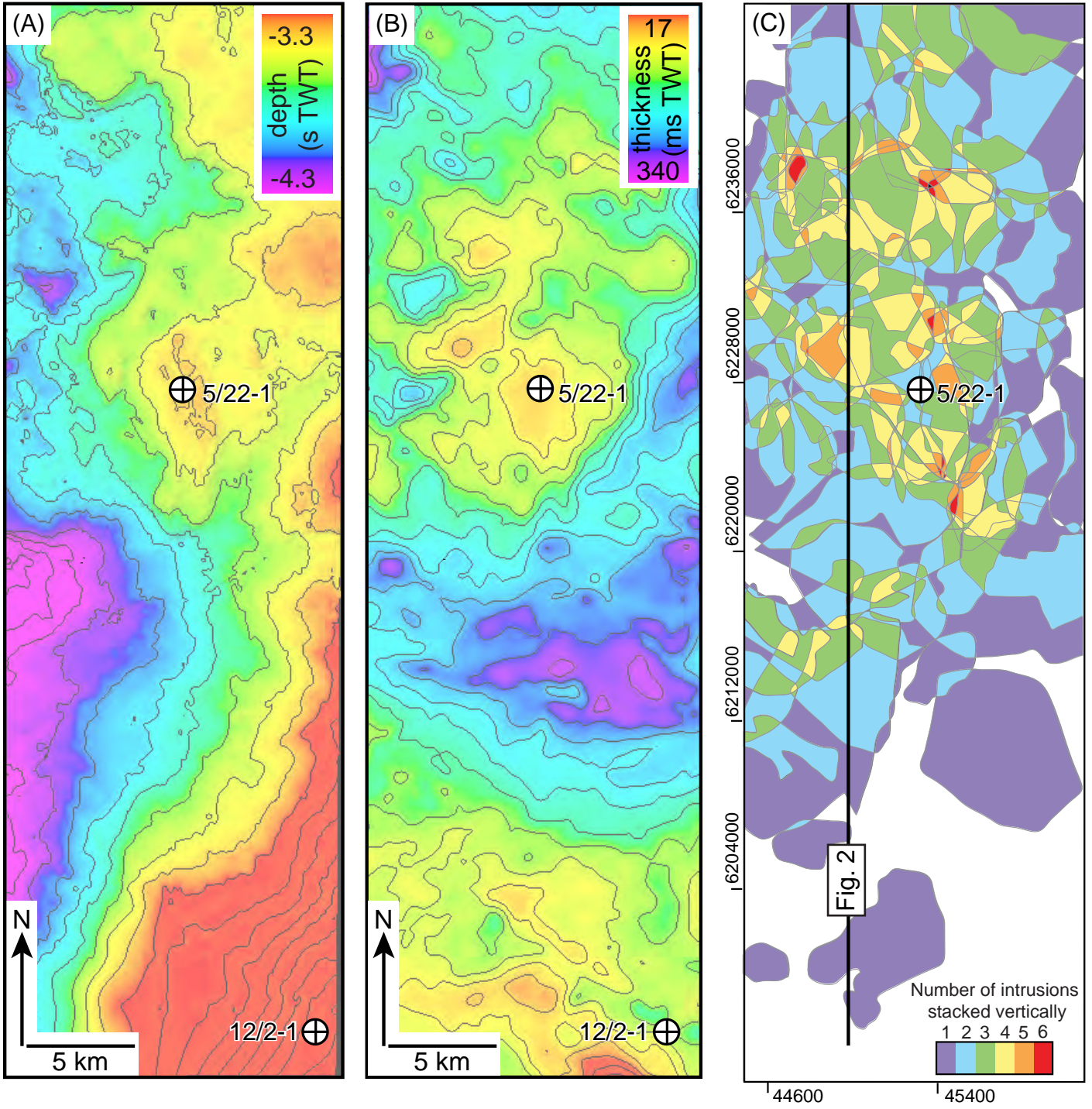


Fig. 6

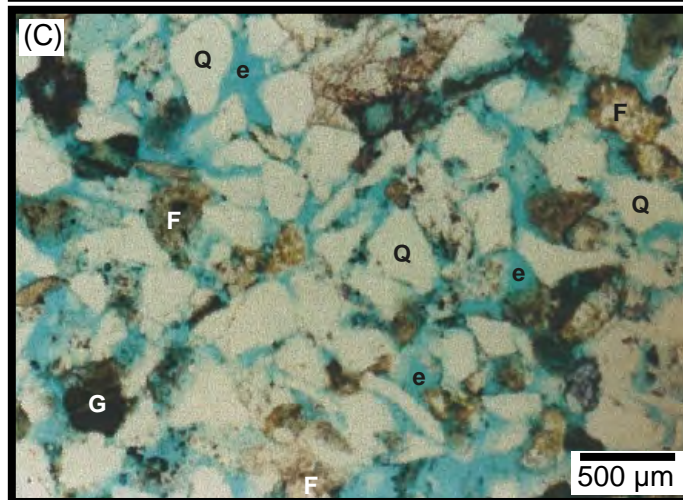
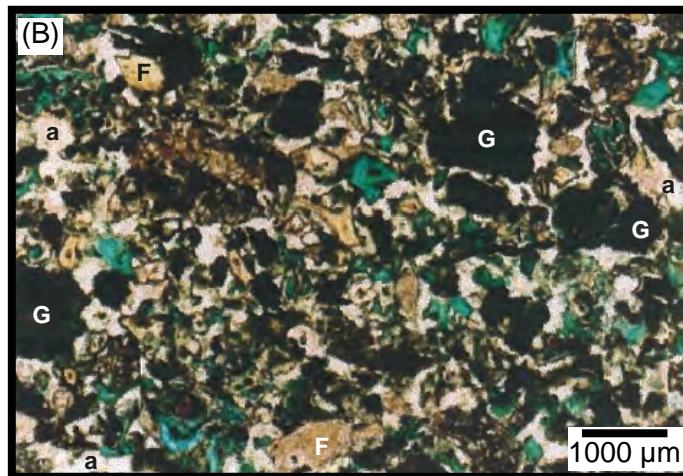
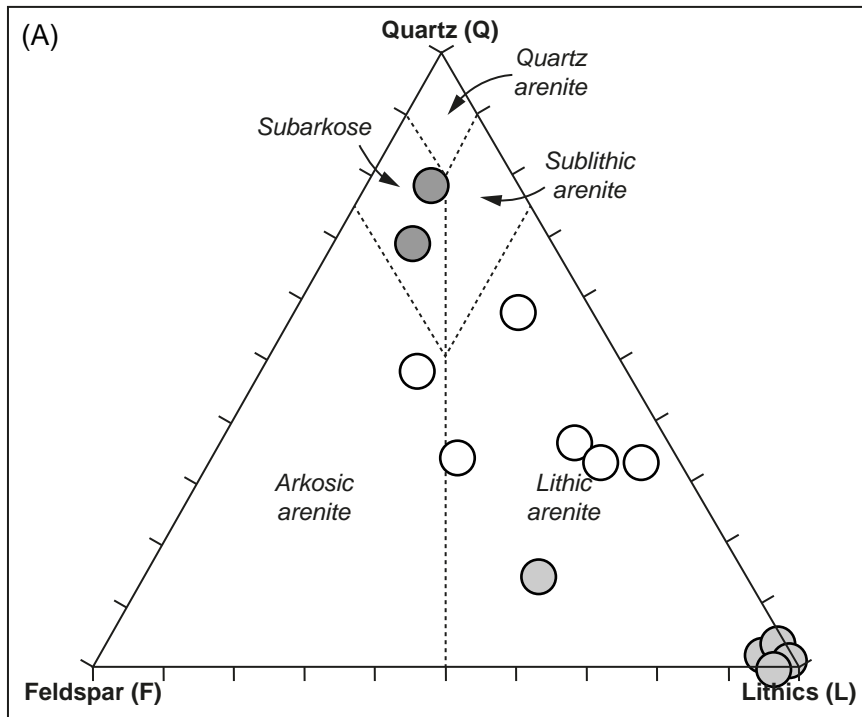


Fig. 7

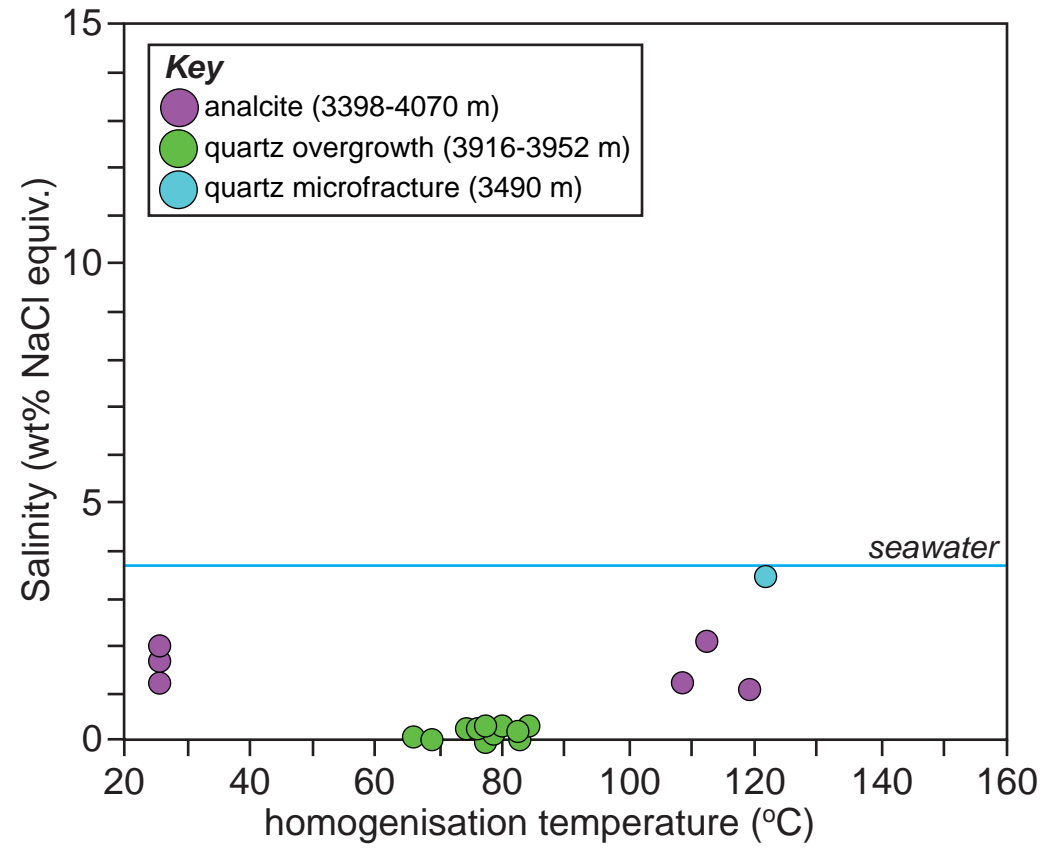


Fig. 8

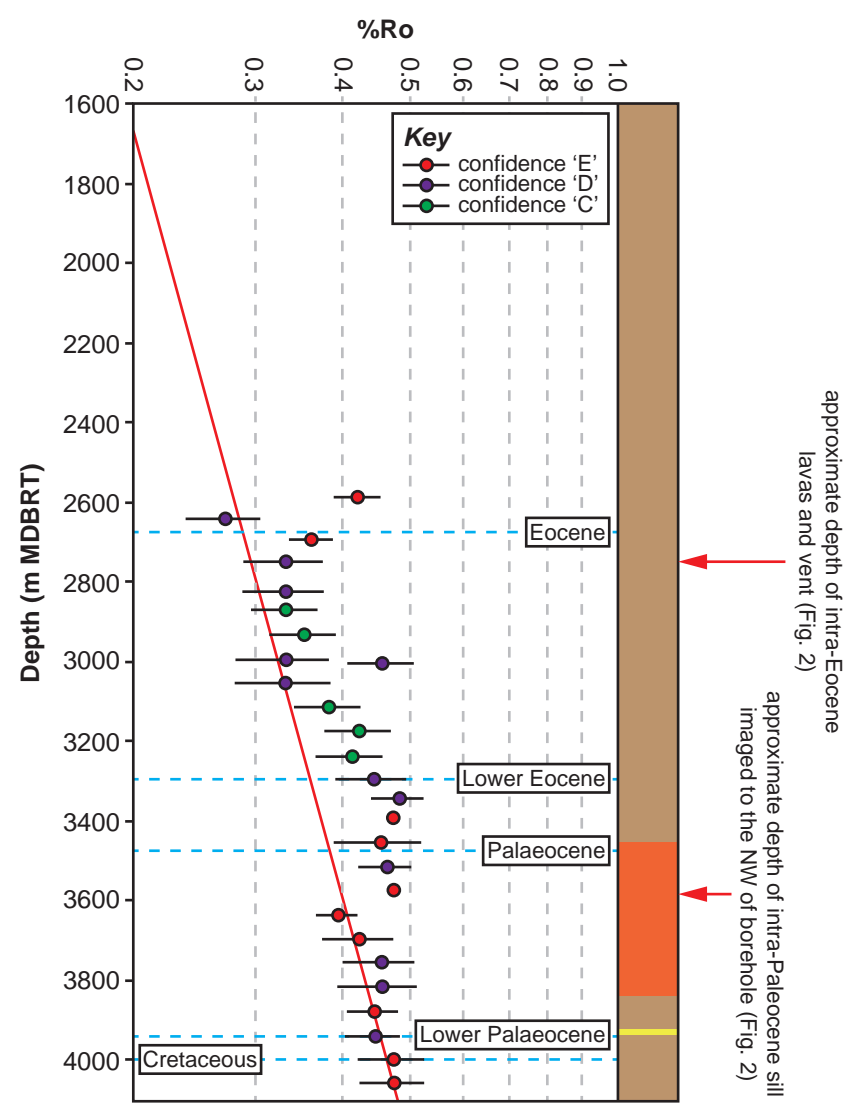


Fig. 9

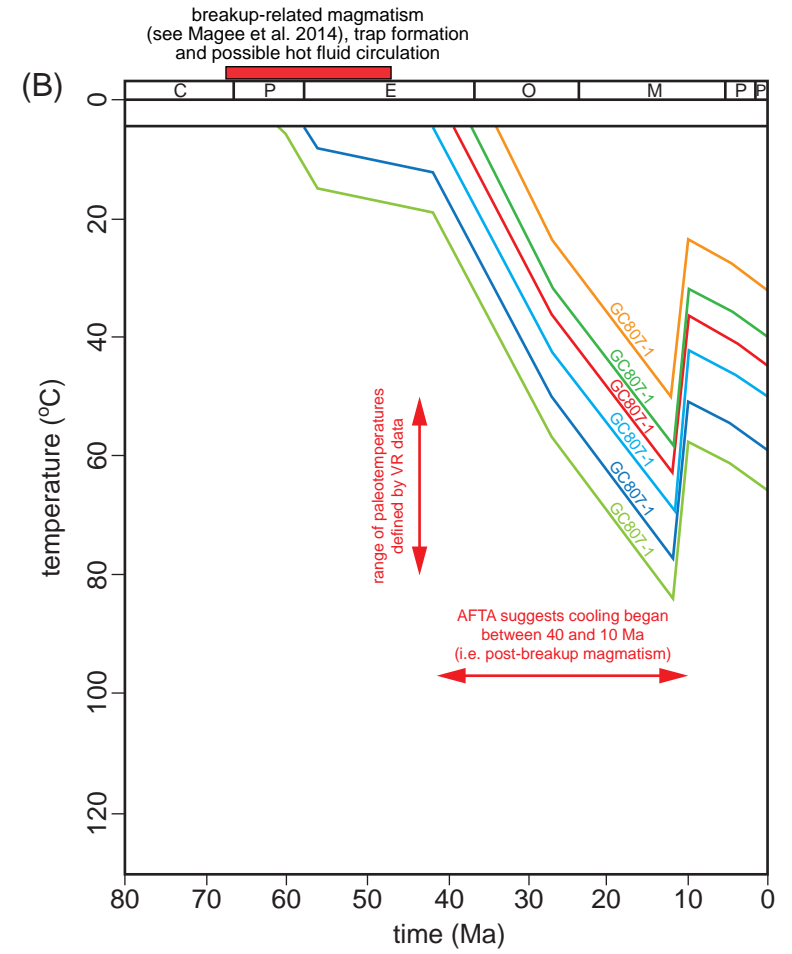
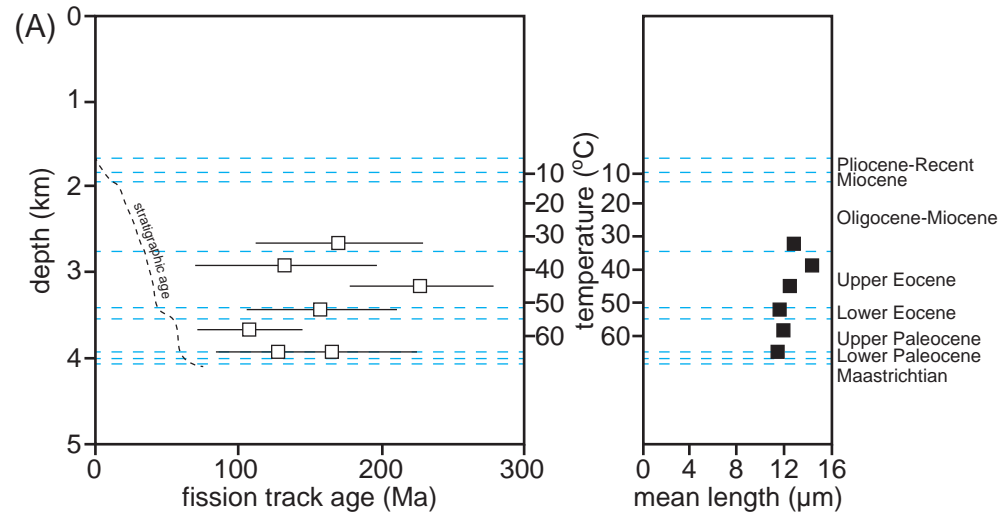


Table 1

Average Depth (m)	Present temperature (°C)	Stratigraphic age (Ma)	Measured VR (%)	Number of readings	Maximum paleotemperature (°C)
2589	29	35-16	0.42	3	70
2643	31	35-16	0.27	7	<50
2697	32	35-16	0.36	4	59
2751	34	35-16	0.33	8	50
2823	36	42-35	0.33	20	50
2871	37	42-35	0.33	20	50
2931	38	42-35	0.35	20	56
2991	40	42-35	0.33	20	50
3051	42	42-35	0.33	20	50
3111	43	42-35	0.38	20	63
3171	45	42-35	0.42	20	70
3231	46	42-35	0.41	20	69
3291	48	42-35	0.44	20	74
3339	49	42-35	0.48	20	80
3387	50	42-35	0.47	1	79
3450	52	56-42	0.45	13	76
3510	54	56-42	0.46	14	78
3570	55	56-42	0.47	1	79
3630	57	60-56	0.39	3	65
3690	59	60-56	0.42	4	70
3750	60	60-56	0.45	13	76
3810	62	60-56	0.45	17	76
3870	63	60-56	0.44	4	74
3930	65	65-60	0.44	11	74
3990	66	65-60	0.47	3	79
4050	68	74-65	0.47	2	79

Table 2

Sample number	Mean depth (mkb)	Stratigraphic age (Ma)	Present temperature (°C)	Maximum paleotemperature (°C)	Onset of cooling (Ma)
GC807-1	2671	42-16	31	<100	post-depositional
GC807-2	2925	42-35	38	<110	post-depositional
GC807-3	3175	42-35	45	60-90	post-depositional
GC807-4	3438	60-35	52	80-100	post-depositional
GC807-5	3688	60-56	58	75-90	40-0
GC807-6	3936	74-56	65	75-100	post-depositional
GC807-7	3936	74-56	65	80-100	>10
				Overlap:	40-10